Journal of Volcanology and Geothermal Research 472 (2026) 108561

Contents lists available at ScienceDirect

Journal of Volcanology and Geothermal Research

journal homepage: www.journals.elsevier.com/journal-of-volcanology-and-geothermal-research

The petrogenesis of Þingmúli volcano, East Fjords, Iceland

Amanda L. Hughes [a,b,*], Joaquín A. Cortés [a], Dave McGarvie [c], Richard J. Moscati [d], Valerie Olive [e]

[a] Department of History, Geography and Social Sciences, Edge Hill University, Ormskirk L39 4QP, UK
[b] Department of Health, Innovation, Technology and Science, Liverpool John Moores University, Liverpool L3 2AJ, UK
[c] Lancaster Environmental Centre, Lancaster University, Lancaster LA1 4YQ, UK
[d] U.S. Geological Survey, Denver Federal Center, MS 963, Denver, CO 80225, USA
[e] Scottish Universities Environmental Research Centre, University of Glasgow, Scottish Enterprise Technology Park, East Kilbride, Glasgow, United Kingdom

ARTICLE INFO

Keywords:
Þingmúli volcano
Iceland
Basalt
Rhyolite
Magma differentiation
Fractional crystallisation
Partial melting
Magma mixing

ABSTRACT

In this work we revisit Þingmúli volcano (Þ = Th), a classic locality known as an example of a complete tholeiitic differentiation. Þingmúli is a ~ 9.5 Ma extinct central volcano located in the East Fjords of Iceland, in which the whole compositional spectrum from basalt to rhyolites have erupted. These volcanic products have been previously considered as petrogenetically related by an ideal fractionation trend, regardless any temporal relationship or volumetric considerations.

Here we report new whole-rock geochemistry, mineral chemistry, isotope analyses, estimation of residence times of the different eruptive deposits, and an update of the original petrogenetic model. Our results highlight that an enriched source, likely spinel lherzolites, generated transitional-alkaline basaltic melts after 15–20% of partial melting at depths of 40–45 km. Many of these basaltic melts erupted at various stages of the volcano's history, while others remained longer in the volcanic plumbing system. These evolved by fractional crystallisation into basaltic andesite magmas with a residence time of ~5 years based on the crystal size distribution of the plagioclase population. Isotopic differences between the basalts/basaltic andesites ($^{87}Sr/^{86}Sr$ ~ 0.7034; $^{143}Nd/^{144}Nd$ ~ 0.51315) and the erupted rhyolites ($^{87}Sr/^{86}Sr$ ~ 0.7037; $^{143}Nd/^{144}Nd$ ~ 0.51304) indicate that the latter are not petrogenetically related to the former. Therefore, instead of a fractional crystallisation mechanism to generate the rhyolites, we propose the partial melting of ignimbrite layers located beneath the volcano. The broad range of trace element concentrations in andesites and dacites and their different isotopic values compared to the basalts strongly suggest that these magmas have been generated by magma mixing between basaltic and rhyolitic melts, similar to modern day Icelandic volcanoes such as Hekla. These results highlight the need to revisit previously studied Icelandic classic localities and reassess their traditionally proposed petrogenetic models.

1. Introduction

Magmatism in Iceland is the consequence of the decompression of the depleted mantle at the Mid Atlantic Ridge (MAR), in conjunction with a thermal anomaly linked to the Icelandic mantle plume (Lawver and Müller, 1994; and references therein). The interplay of both sources produces three distinct magma compositions defined as three distinctive magma series upon differentiation (e.g., Jakobsson et al., 2008): tholeiitic (magmas with a lower concentration of alkalis and titanium and a high proportion of iron and magnesium per amount of SiO_2), alkaline (magmas with a higher concentration of alkalis and lower proportion of iron and magnesium per amount of SiO_2 compared to tholeiites), and transitional alkaline, i.e., an intermediate series between the other two.

Although volcanic products in Iceland are predominantly basalts, which dominate both intrusive suites and extrusive sequences at central volcanoes (Icelandic volcanoes which host a long-lived crustal magma reservoir, e.g., Thordarson and Larsen, 2007), it has long been established that most central volcanoes are bimodal basalt-rhyolite systems (e.g., Bunsen, 1851; Walker, 1966), with scarce basaltic andesite, andesitic and dacitic compositions. However, there are several central volcanoes containing significant volumes of intermediate (i.e., basaltic

* Corresponding author at: Department of Health, Innovation, Technology and Science, Liverpool John Moores University, Liverpool L3 3AF, UK
E-mail address: A.L.Hughes@ljmu.ac.uk (A.L. Hughes).

https://doi.org/10.1016/j.jvolgeores.2026.108561
Received 16 September 2025; Received in revised form 23 January 2026; Accepted 6 February 2026
Available online 9 February 2026

andesite to dacite) compositions in addition to rhyolites and basalts, and these provide an opportunity to shed light on the petrogenetic processes generating rhyolitic magmas in Iceland, which have traditionally been modelled by fractional crystallisation (e.g., Lacasse et al., 2007; Thordarson and Larsen, 2007). One of these central volcanoes with a significant volume of basaltic andesites, andesites and dacite lavas is Þingmúli, which is considered a classic example of a tholeiitic differentiation trend by fractional crystallisation (Carmichael, 1962; Charreteur et al., 2013).

Þingmúli is an extinct central volcano in Eastern Iceland, located ~11 km west of Reyðarfjörður central volcano (Fig. 1). Its eroded remnants rise ~1200 m asl and are heavily dissected by glacial valleys and fluvial channels. The central volcano's age has been estimated at ~9.5 Ma based on the correlated ages of nearby flood basalt sequence thickness (Charreteur et al., 2013), but a radiogenic isotope age for Þingmúli itself does not exist. Þingmúli is underlain by volcanic sequences from Reyðarfjörður (Helgason and Zentilli, 1982), and Tertiary flood basalts deposited during Iceland's formation (e.g., Walker, 1957). Eruptions at Þingmúli range from effusive to fountaining basaltic eruptions, fissure eruptions, to explosive rhyolitic eruptions, generating coulées and pyroclastic flows (Hughes, 2025).

The volcanic sequence at Þingmúli contains a full compositional tholeiitic trend from basalt to rhyolite, and the volumetric proportions of each composition are estimated at 66 vol% basalts, 9 vol% combined basaltic andesites, andesites and dacites, and 25 vol% rhyolites. Previously published studies from Carmichael (1962, 1964) and Charreteur et al. (2013) interpreted these compositions as the result of a fractional crystallisation-driven evolution, using picrites as the parental magma that evolved up to high-silica rhyolites (HSR; SiO_2 over 75 wt% on a dry basis). The compositional trend also displays a relative iron enrichment, accounting for the occurrence of iron-rich basalts (ferro-basalts) and iron-rich andesites (also known as icelandites; Carmichael, 1967). The compositional trend at Þingmúli has since become a textbook example of the tholeiitic differentiation (e.g., Carmichael et al., 1974; Hughes, 1982; Wilson, 1989) and has been used as a reference to characterise other tholeiitic trends elsewhere (e.g., Franceschelli et al., 2005; Frost and Frost, 2022).

The aim of this study is to re-evaluate the fractionation-driven

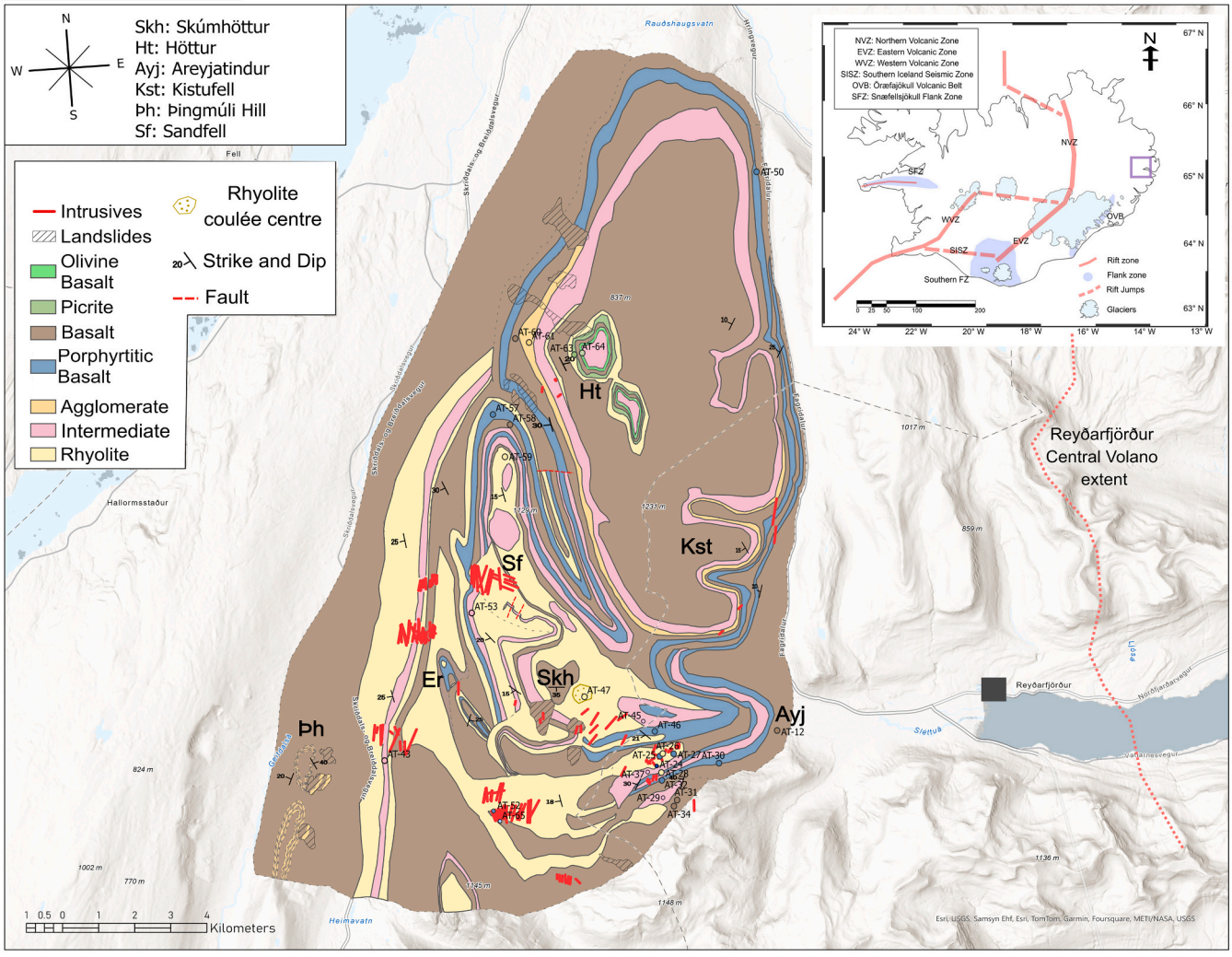

Fig. 1. a) Geology of Þingmúli Central Volcano with five key summit names labelled. Units given in the legend have been classified by field mapping, using textural and mineralogical differences. Samples from this study are indicated as AT-XX. For the purposes of this study, picrite, olivine basalt, porphyritic basalts and agglomerate shown in the map are grouped with basaltic lavas in the text. Intermediate refers to basaltic andesite, andesite and dacite lavas. Black hashed areas mark regions of landslides/slope failures. The extent of the nearby Reyðarfjörður central volcano is given by red dotted line (Askew, 2020) as an important source for some of the pyroclastic layers under Þingmúli. Inset shows Þingmúli in relation to Iceland, with volcanic zones, location of rift and flank zones marked on. Blue regions mark current flank zones, while the red line marks the location of the Mid Atlantic Ridge. Dotted lines mark regions of rift jumps, where the rift zones have moved to align with the mantle plume. Current centre of the mantle plume is given by red star. Inset after Einarsson and Sæmundsson (1987). (For interpretation of the references to colour in this figure legend, the reader is referred to the web version of this article.)

tholeiitic differentiation model proposed at Þingmúli, and to investigate alternative petrogenetic processes (i.e., partial melting and magma mixing) that may account for the occurrence of its full compositional trend (i.e., basalt to rhyolite). We also compare Þingmúli and its products with other currently active central volcanoes that display full compositional trends such as Hekla.

2. Methods

2.1. Field Work and Sample Strategy

Fieldwork at Þingmúli took place between the 1st and 19th July 2022, for the collection of stratigraphically constrained samples, geological mapping, and the stratigraphic logging of the different volcanic products to establish their erupted volumes and Þingmúli's temporal evolution. Fieldwork was concentrated in the Areyjardalur valley, where a nearly complete exposed sequence outcrops, but also included the study of the basic stratigraphic of all the main summits in the area.

Sampling and logging areas were determined prior to fieldwork, based on the locations of previously collected samples (Charreteur et al., 2013), aerial imagery and pre-existing geological maps (Walker, 1957; Carmichael, 1962; Charreteur et al., 2013) to target the areas where most units outcrop and occur in a stratigraphic order, which can be logged. The field season was split according to area importance, with most time allocated for sample collection, mapping, and logging in the Areyjardalur valley. The valley was logged and mapped for a total of 4 days, with 6 logs completed along the valley.

Geological mapping took place throughout the field season, using lithological contacts derived from logging, and field observations of sample sites. In areas of limited accessibility, aerial imagery was used to aid in mapping and identifying probable outcrops and contacts. Key areas for detailed mapping were chosen at Sandfell, Skúmhöttur and Þingmúli hill (Fig. 1), to complement previous mapping (e.g., Carmichael, 1962). Similarly, samples were collected in areas of stratigraphic importance and areas in which there was limited previous sampling to best complete geochemistry of all units in the complex.

2.2. Whole-rock chemistry

Twenty-four samples were selected for whole-rock chemical analyses (Table S1: Supplementary data). Major and trace elements were analysed using the Panalytical PW2404 X-ray fluorescence (XRF) instrument hosted at the School of Geosciences, The University of Edinburgh. The rock samples were ground to a fine powder of around 120 μm using a tungsten carbide mill.

Major element concentrations were measured on 40 mm-diameter fused glass discs; about 0.9 g of sample powder was mixed with a borate flux using a 5:1 flux:sample dilution following the procedure summarised in the supplementary information. Thereafter, the samples were fused and heated in Pt-5% Au crucibles at 1100 °C.

Rare earth element concentrations (Table S1) were measured in the same 24 samples by inductively coupled plasma mass spectrometry (ICP-MS). The analytical procedure is detailed in Olive et al. (2001), whereby dissolution of 0.1 g of sample powder was achieved by three-acid digestion (HF, HNO_3, HCl), followed by $HClO_4$ digestion to avoid the formation of insoluble fluorite and to ensure dissolution of spinel phases. Analyses were performed on the Agilent 7500ce ICP-MS instrument at the Scottish Universities Environmental Research Centre (SUERC) using the USGS BCR2 standard (Wilson, 1997) as calibration. Samples from this study were then merged in a database alongside analyses from Carmichael (1962, 1964) and Charreteur et al. (2013).

2.3. Petrography and mineral chemistry

A total of 34 samples were collected for conventional optical petrography. Further petrography was carried out on back scattered electron (BSE) images taken in a JEOL IT700HR scanning electron microscope equipped with a JEOL energy dispersive spectroscopy (EDS) detector, housed at Edge Hill University. Semiquantitative mineral chemistry (Table S2: Supplementary material) of the main mineral phases was also measured in these samples using the EDS detector. The collected BSE images were taken with an overlap of 10% between them and studied using FIJI (Schindelin et al., 2012) in which ellipses were drawn manually around plagioclase feldspar phenocrysts to obtain, using FIJI's built-in functions, the maximum and minimum axes of each individual crystal to determine the crystal size distribution (CSD) of the crystal population. Over 300 measurements were collected in each thin section (extra care was taken to avoid double-measuring a crystal in the overlap between the images), to have a representative sample of the plagioclase CSD from each outcrop layer (Morgan and Jerram, 2006). CSDslice (Morgan and Jerram, 2006) was used to estimate the 3D crystal aspect ratios based on the 2D axes measured on thin sections. Data were then exported into CSDCorrections 1.61 (Higgins, 2000). Additional parameters needed to calculate the CSD of a crystal population such as the phase volume and vesicularity were estimated directly by visual inspection from conventional petrography, while the total thin section area was measured by the addition of the individual field of view areas of the used thin section microphotographs using FIJI's measuring tools. The CSD of the mineral phase was also used to estimate the residence time of its crystal population based on the following relationship (Marsh, 1988):

$$t_r = \frac{-1}{mG_R}, \quad (1)$$

in which t_r is the residence time of the crystal population, G_R is the growth rate of the mineral phase and m is the slope of its CSD.

In addition to samples collected in this study (denoted by AT-XX in the Supplemental Tables), 18 petrographic samples from Carmichael (1962) have been re-described. The description of these samples is included with the general petrographic overview.

Mineral chemistry data reported in this study include new data obtained using the method above (denoted by AT-XX), and from Charreteur (2012). Data from Charreteur (2012) follow the format 0X0X-XX, or TX-0X.

2.4. Isotopic Chemistry

Seven samples, representative of the different rock compositions, and of the generic stratigraphic sequence found at Þingmúli, were selected for radiogenic isotopic analyses ($^{87}Sr/^{86}Sr$, $^{143}Nd/^{144}Nd$, $^{206}Pb/^{204}Pb$, $^{207}Pb/^{204}Pb$ and $^{208}Pb/^{204}Pb$). Whole-rock, single-dissolution, isotope geochemistry, followed by thermal ionization mass spectrometry (TIMS) were conducted at the United States Geological Survey (USGS) in Denver. Samples were analysed using an Isotopx Phoenix™ 9-collector TIMS for Nd, operating with an 8 kV acceleration voltage and 10^{11} Ω resistors for the Faraday cups. Neodymium was also run in dynamic mode if enough material allowed. Strontium and Pb were analysed in static mode with a ThermoFinnigan Triton™ multi-cup TIMS fitted with a single electron multiplier for ion counting. The detailed procedure is given in the Supplementary Information.

3. Results

3.1. Whole rock geochemistry

Re-examination of the whole-rock geochemistry of the Þingmúli lavas reveals that the sequence is closer to the transitional alkaline series in a Total Alkali vs Silica (TAS) diagram (Fig. 2a) than the tholeiitic series, with most basaltic samples containing higher total alkali concentrations than the average tholeiite at the same SiO_2 concentration (e.g., Zimmer et al., 2010). Although the majority of the sequence is in the

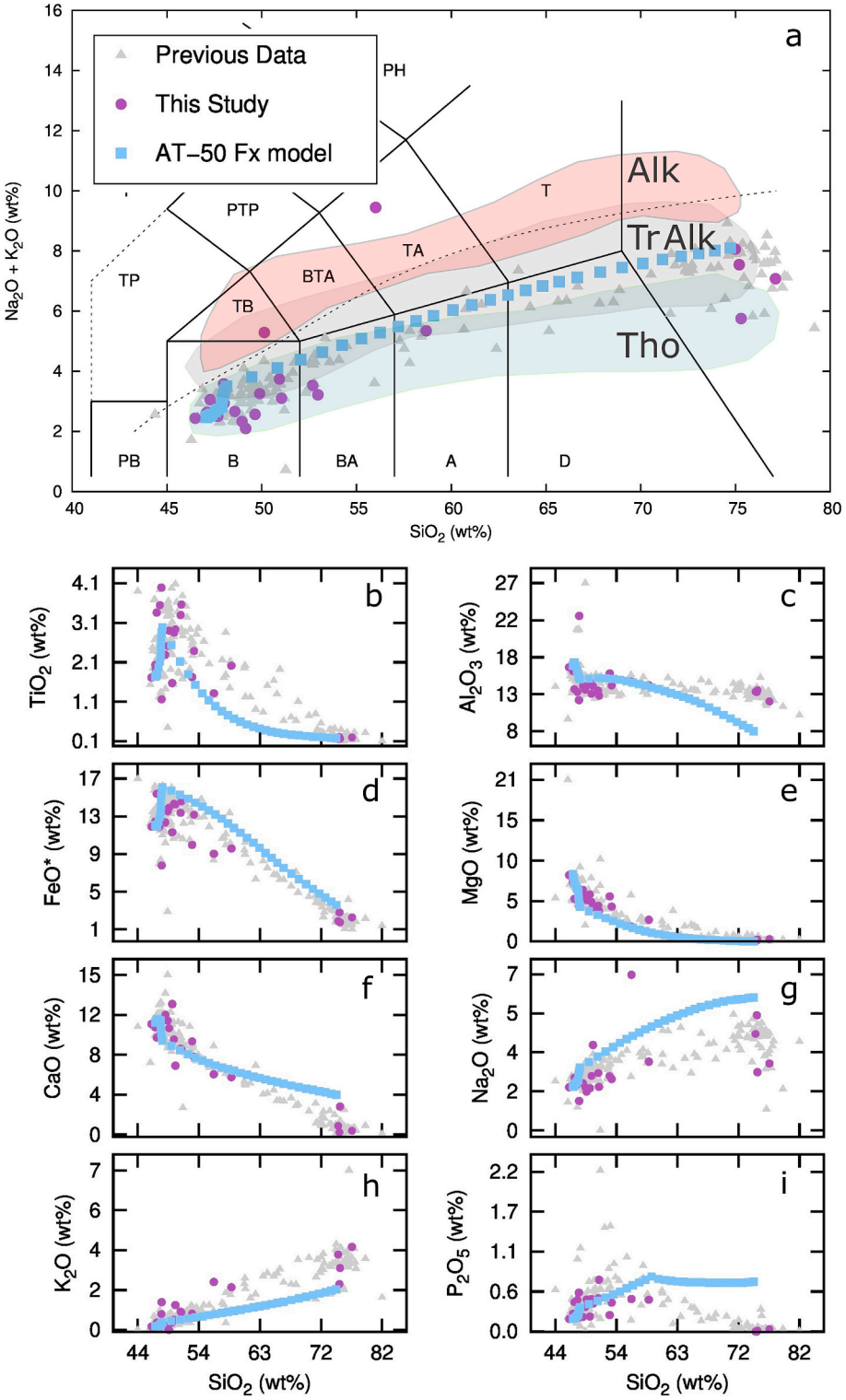

Fig. 2. Major element characteristics of the Þingmúli volcanic sequence. a) TAS diagram (Le Maitre et al., 1989) displaying compositions at Þingmúli, which plot within the transitional alkaline (Tr Alk; pale yellow) field in the sense of Jakobsson et al. (2008); dashed line marks Irvine and Baragar (1971) boundary between the alkaline and sub-alkaline fields. Published data (grey triangles) from Carmichael (1962, 1964) and Charreteur et al. (2013), this study data magenta circles. b) TiO_2 vs SiO_2, c) Al_2O_3 vs SiO_2, d) FeO* vs SiO_2, e) MgO vs SiO_2, f) CaO vs SiO_2, g) Na_2O vs SiO_2, h) K_2O vs SiO_2, i) P_2O_5 vs SiO_2 variation diagrams for the lithologies at Þingmúli; symbols as in Fig. 2a. (For interpretation of the references to colour in this figure legend, the reader is referred to the web version of this article.)

transitional alkaline field, few basalts contain lower alkali concentrations and plot in the tholeiitic field, with one outlier sample plotting in the trachyandesite field.

Figs. 2a to 2i also display for comparison an ideal fractional crystallisation trend (in light blue; see Table S7b) calculated using rhyolite-MELTS (Gualda et al., 2012; Asimow and Ghiorso, 1998; Ghiorso and Sack, 1995), starting from the composition of basalt AT-50 (our most primitive sample with 46.27 wt% of SiO_2 and 8.42 wt% of MgO), at pressures of 100 MPa, consistent with the average location of shallow magma reservoirs in many current active central volcanoes (Ofeigsson

et al., 2011; composition and full set of conditions in supplementary Table S5). The trend fairly reproduces the compositions from basalt to basaltic andesites, but it becomes less precise with intermediate and rhyolitic compositions. The calculated fractional crystallisation trends are curved for several elements (e.g., TiO_2, Al_2O_3, CaO), which does not match the near-linear compositional distribution displayed by the samples.

On the major elements vs SiO_2 wt% variation diagrams (Figs. 2b-i), basalts increase from 2 to 4 wt% in the TiO_2 wt% vs SiO_2 wt% diagram (Fig. 2b) and from ~9 to 15 wt% in the FeO* vs SiO_2 wt% diagram

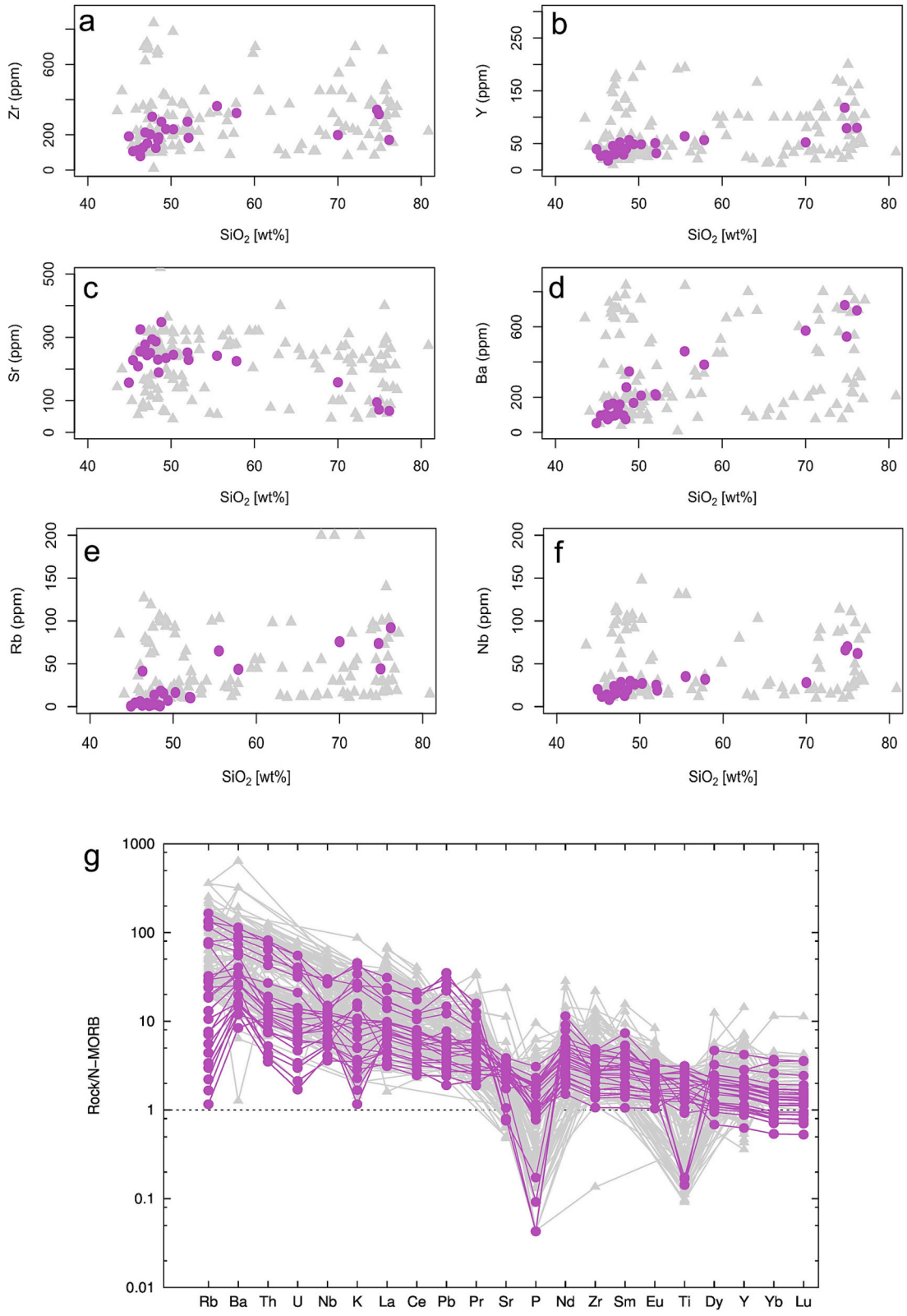

Fig. 3. Trace element characteristics of the Þingmúli volcanic sequence. a-f) Variation in selected trace elements vs SiO_2 diagram for the lithologies at Þingmúli. g) spider diagrams for Þingmúli's basalts, normalised to N-MORB from Sun and McDonough (1989). Colours and symbols as in Fig. 2a.

(Fig. 2d), with SiO_2 increasing from 46 to 50 wt%, which is consistent with a reduced conditions fractionation trend (e.g., Cottrell et al., 2021). At more evolved compositions, the trend show a decrease in TiO_2, FeO*, MgO and CaO and increase Na_2O and K_2O with increase SiO_2, however a trend following a theoretical liquid line of decent is no longer clear. The most evolved magma compositions reach 82 wt% SiO_2 i.e., High Silica Rhyolites (HSR; Gualda and Ghiorso, 2013).

Trace elements vs SiO_2 wt% variation diagrams (Fig. 3a-f) show the basaltic lavas contain higher concentrations of incompatible elements such as Zr and Y compared with an average tholeiitic basalt (e.g. Sun and McDonough, 1989), with concentrations of 200 and 50 ppm respectively. A small group of basalts and basaltic andesites show even higher concentrations (approx. 700 ppm Zr and 150 ppm Y, Fig. 3a and b respectively), similar to concentrations of oceanic island basalts (OIB) produced by mantle plumes (Sun and McDonough, 1989). Interestingly, all trace elements show little or no correlation with SiO_2; for example, Zr concentrations vary between 200 and 400 ppm (Fig. 3a) and Y concentrations vary between 0 and 100 pm (Fig. 3b) regardless of the silica content. Using fractional crystallisation proxies such as Sr (for plagioclase fractionation) again reveals uniform concentrations between 100 and 300 ppm (Fig. 3c) regardless of silica content. In a spider diagram normalised to N-MORB (Fig. 3g; Sun and McDonough, 1989), minor enrichment of large ion lithophile elements is observed with depletions in P_2O_5 and TiO_2.

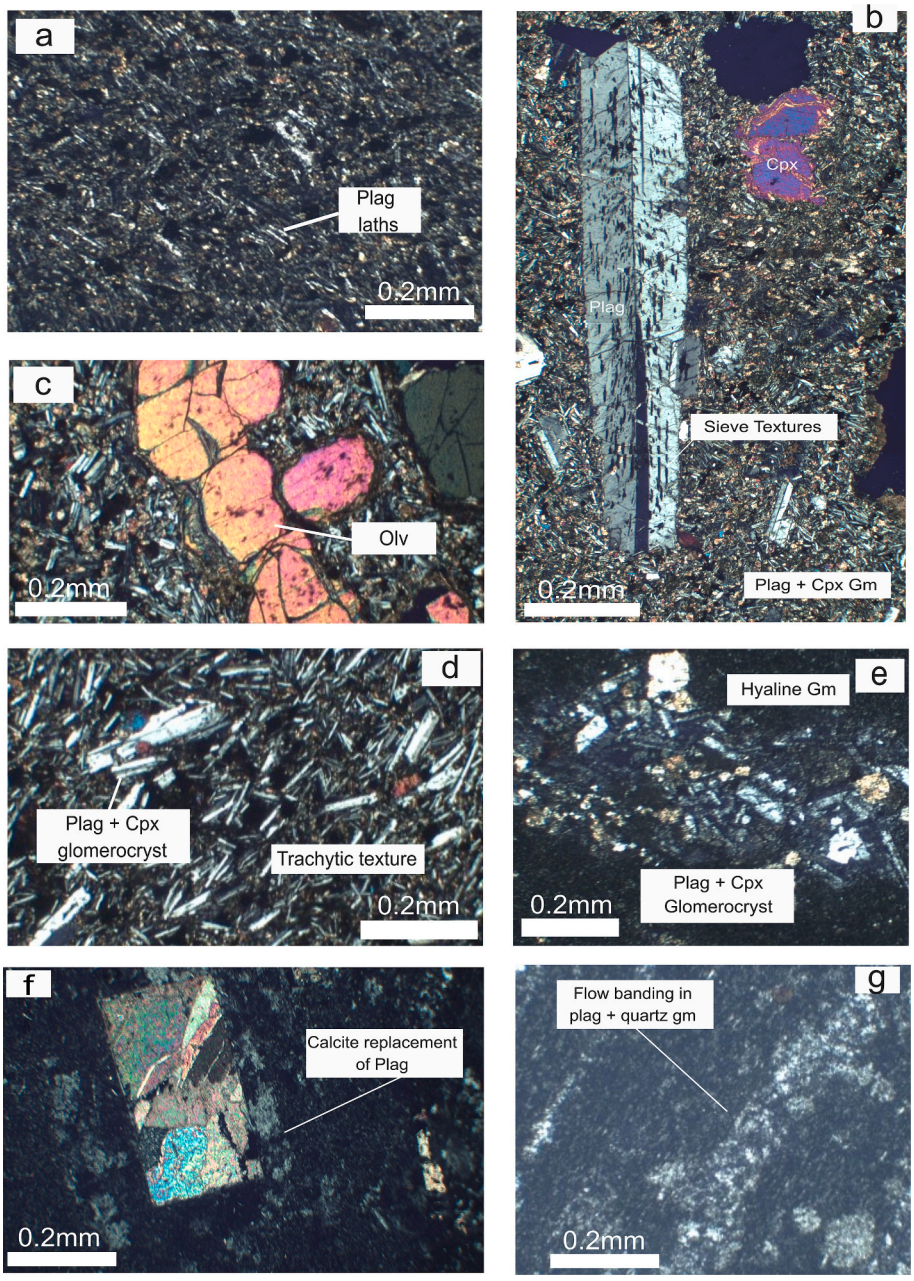

Fig. 4. Photomicrographs images of the Þingmúli lavas. a) The trachytic texture of an aphanitic basalt lava (AT-12) with plagioclase (Plag) laths as the main mineral mode. b) A sample of porphyritic basalt (in a sample from Carmichael, 1962), with a 0.8 mm plagioclase phenocryst exhibiting sieve textures within a plagioclase and clinopyroxene (Cpx) groundmass. c) An olivine (Olv) phenocryst within a picrite lava from Carmichael (1962). d) and e) Show plagioclase and clinopyroxene glomerocrysts within andesite lava flows in sample AT-43, (d) With trachytic texture in a sample from Carmichael (1962), and (e) With hyaline groundmass in sample AT-45. f) Shows textures in rhyolitic lavas, with the replacement of plagioclase phenocrysts by calcite in a sample from Carmichael (1962). g) Quartz microlites in flow bands in sample AT-47. Graphical scale in white is indicated on each photomicrograph.

3.2. Petrography

In the following petrographic descriptions, we consider phenocrysts as those crystals in which the longest axis is greater than 0.5 mm, while microcrysts are crystals up to 0.2 mm.

3.2.1. Basalts (aphanitic and porphyritic)

3.2.1.1. Aphanitic basalts. A total of 11 samples were described, including 9 from this study and 2 redescribed from Carmichael (1962). Basalts are holocrystalline with a fine grained (avg. 0.5 mm) groundmass. In some cases, they exhibit alignment of crystals in a trachytic texture (Fig. 4a). Plagioclase is the main mineral phase in the basaltic lavas (50–60 vol%), with 0.3–1 mm laths commonly appearing in the groundmass, and rare phenocrysts up to 2 mm in size. Crystals are typically labradorite to andesine in composition (~An_{50} to An_{69}). Clinopyroxene (30 vol%) is found in the groundmass of many samples, ~0.3 mm in length. Clinopyroxene is also found as a component of few 1–4 mm glomerocrysts alongside fragmented plagioclase and rare olivine. Oxides, primarily titanomagnetite (2 vol%) and rutile (5 vol%), are found as well-formed euhedral crystals within the groundmass and in some samples are found forming micro-veins, 1 mm in width, which extend across the samples. Olivine is rarely found in aphanitic basalts, with only one sample containing 0.1 mm euhedral crystals. In this particular sample, olivine comprises 15 vol%.

3.2.1.2. Porphyritic basalts. A total of 10 samples were described, 8 from this study and 2 redescribed from Carmichael (1962), one of which is a picrite. The porphyritic basalts are almost 100% holocrystalline with 0.3 mm (average) plagioclase laths within a plagioclase and clinopyroxene groundmass hosting larger (0.5–1.5 mm) crystals of plagioclase, clinopyroxene, and rare olivine. Similar to the aphanitic basalt, plagioclase is the main mineral phase (50 vol%) occurring in both the groundmass as laths, and as euhedral ~0.8 mm phenocrysts with a composition of mainly labradorite (~An_{60} to An_{65}). Plagioclase phenocrysts in all studied samples display sieve textures, which are often aligned within the crystal (Fig. 4b).

Clinopyroxene comprises around 30–40 vol% of the samples found as small 0.2 mm crystals in the groundmass, or as larger 0.6–0.8 mm euhedral phenocrysts, often showing simple twinning. Both clinopyroxene and plagioclase also occur in glomerocrysts in many samples, with 1.5–2 mm fragmented crystals. Olivine (up to 10 vol%) occurs mostly in the groundmass as 0.2 mm euhedral crystals. Oxides, specifically titanomagnetite, rutile, and rare haematite (jointly comprising ~5 vol% of samples) are found as 0.2 mm well-formed euhedral crystals, almost always as groundmass phases.

Picritic lavas (Fig. 4c) have a porphyritic texture with large (up to 1 cm) phenocrysts of olivine and plagioclase held in a fine-grained ~0.1 mm groundmass. Olivine is the most abundant mineral, comprising up to 50 vol% of the samples. The olivine crystals are ~0.8 mm, subhedral, phenocrysts, and are mostly well preserved with only small rim alterations to iddingsite (<1 vol%). Plagioclase is found as both phenocryst and microcrysts in the groundmass (up to 25 vol%), occurring as 0.1 mm laths with no apparent orientation. As phenocrysts plagioclase is well-formed with few crystals displaying sieve textures. Clinopyroxene comprises up to 15 vol% of the samples. It is present in the groundmass, where it forms 0.1 mm euhedral crystals. Oxides in the samples are rare, only making up <5 vol% of the groundmass. These are primarily titanomagnetite and rutile and occur as euhedral crystals.

3.2.2. Basaltic Andesite, Andesite and Dacite Lavas

A total of 8 samples were redescribed, 5 from this study and 3 from Carmichael (1962). Of the 8 samples, 3 are basaltic andesites, 4 andesites and 1 dacite. Samples are mostly holocrystalline with an aphyric to fine- grained groundmass. Where a groundmass occurs, it is made up of fine 0.1–0.2 mm plagioclase laths with euhedral 0.1 mm clinopyroxene microlites. Plagioclase is the main mineral component (up to 60 vol% in samples with a fine groundmass, and up to 10 vol% where samples are hyaline) with plagioclase laths (~An_{70} to An_{75}), often orientated in a trachytic texture (Fig. 4d). Clinopyroxene occurs as small groundmass microlites (5–20 vol%).

Phenocrysts are rare, but when these occur, they are always plagioclase, or glomerocrysts of plagioclase and clinopyroxene (Fig. 4e), and typically display disequilibrium textures such as dissolution rims and sieve textures. Titanomagnetite and haematite are found as 0.1 mm crystals within the groundmass or glass or as alteration. Where samples are hypocrystalline, the main crystals are plagioclase (50 vol%) or glomerocrysts of plagioclase and clinopyroxene.

3.2.3. Rhyolites

A total of 6 samples were described, 4 from this study and 2 from Carmichael (1962). Rhyolite samples range from hyaline to hypocrystalline. Groundmasses are commonly glassy (~60 vol%) but can contain, up to 30 vol% of 0.2 mm plagioclase laths (~An_{21} to An_{35}) interspersed with quartz (up to 10 vol%). Alteration of rhyolite lavas is common (Fig. 4f), with samples containing calcite (6 vol%), chlorite (2%), kaolin (1 vol%) and prehnite (1 vol%). Flow banding occurs in many samples. The bands are typically 1 mm in thickness, and plagioclase and quartz microlites are typically aligned following these bands (Fig. 4g). In previous studies, enclaves of basaltic composition have been found in rhyolites (Charreteur, 2012) suggesting these compositions of magmas interacted with the rhyolitic magmas prior to eruption.

3.3. Mineral chemistry

The most abundant minerals occurring in each lithology (in both groundmass and phenocryst phase) are plagioclase and pyroxene each in an approximate respective abundance of 30–40 vol% in basaltic lavas, 20–30 vol% in andesite and dacite lavas and less than 10 vol% in rhyolitic lavas. Mineral chemistry data are given in supplemental Table S2.

3.3.1. Basaltic lavas

Plagioclase compositions are broadly uniform in the basaltic lavas (Fig. 5a), spanning mostly bytownite to andesine (~An_{50} to An_{70}), with averages close to labradorite (~An_{55}). Sample AT-12 contains the largest spread of plagioclase compositions, with few phenocrysts reaching the andesine-oligoclase boundary Fig. 5a). Plagioclase rims and cores show limited variation, with cores clustering around the labradorite-bytownite boundary, and rim measurements around labradorite-bytownite/andesine. This normal zoning is suggestive of growth in a continually evolving magma. Sample AT-32, a porphyritic basalt, shows a single plagioclase population with albitic composition, which we interpret as the result of hydrothermal alteration (e.g., Carmichael, 1962). This is supported by kaolinization on plagioclase crystals identified in thin sections.

Pyroxenes in the basaltic lavas are mainly augite, with compositions spreading from low-Ca monoclinic pyroxenes (pigeonite) up to diopside (Fig. 5a). Samples AT-12, AT-32, AT-35 and AT-64 contain mainly clinopyroxene with minor occurrences of orthopyroxene. The Mg# for all analyses range from 50 to 88, with an average of 70.

3.3.2. Basaltic Andesite, Andesite and Dacite lavas

Plagioclase mineral chemistry (Fig. 5b) in these lavas is biased as only one sample from this study could be measured (AT-49) with another published in the literature (0309–04; Charreteur, 2012). Regardless, the compositional extent is broadly similar to those found in the basaltic lavas, with bytownite (~An_{72}) found in sample AT-49 and andesine-labradorite (~An_{48}) found in sample 0309–04 (Charreteur, 2012). Pyroxenes in both samples are similar to those found in basaltic samples, spanning diopside-augite compositions, with Mg# ranging

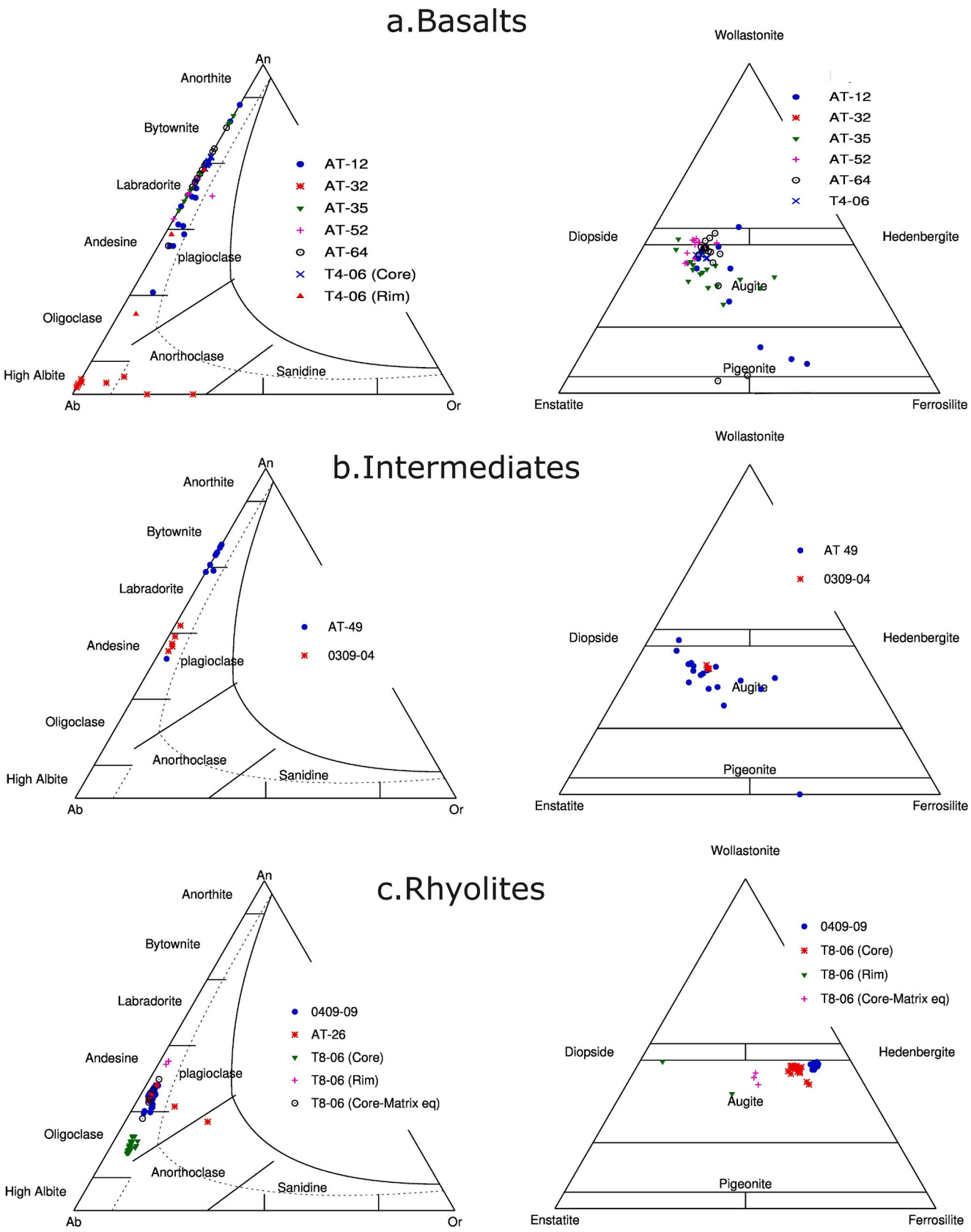

Fig. 5. Mineral chemistry of plagioclase and pyroxenes in (a) basaltic lavas, (b) basaltic andesite, andesite and dacite lavas and (c) rhyolitic lavas. For each classification plot a key is given. AT-XX samples are those generated in this study. 0X09-0X/TX-0X data are taken from Charreteur (2012).

from 65 to 72 in phenocrysts in sample AT-49, common to 0309–04 (Charreteur, 2012), with Mg# = 67–70. Olivine phenocrysts found in sample AT-49 have Fo% average values close to 60%.

3.3.3. Rhyolite lavas

Fresh (i.e., unaltered) crystals are relatively scarce in the rhyolites due to their high level of hydrothermal alteration over Þingmúli's lifespan (Carmichael, 1962). The sample T8–06; Charreteur, 2012), contains plagioclases with variable core-rim compositions (Fig. 5c). Cores have on average oligoclase compositions (~An_{19}), while rims have on average andesine compositions (~An_{45}). Rims of pyroxenes found in T8–06 have Mg# ~60 and plot toward diopside-augite boundary, with the equilibrium between cores and matrix being augite. Mg# ~ 46. Mg# in cores varies between 20 and 30 with few crystals of clinopyroxene found in sample 0409–09 with a composition close to hedenbergite, with Mg# of 16–20 (Fig. 5c).

3.4. Plagioclase crystal size distribution

At Þingmúli, nucleation rates of plagioclase are unknown. Growth rates were chosen based on Brugger and Hammer (2010) work, which include growth rates for plagioclase based on situational occurrence, i.e., slow intrusive cooling (between 10^{-10} and 10^{-8} mm s^{-1}) vs *syn*-eruptive microlites (between 10^{-6} and 10^{-8} mm s^{-1}) crystallisation. Since basaltic andesites, based on geochemistry, are thought to be the product of fractional crystallisation, the largest growth rate was chosen (10^{-10} mm s^{-1}), and basaltic samples were assigned a growth rate of 10^{-8} / 10^{-7} mm s^{-1} dependent on crystal size, which gave an indication of *syn*-eruptive crystallisation. Brugger and Hammer (2010) also includes a growth rate for ascending andesites, (10^{-7} mm s^{-1}), which was used to calculate residence time of the smaller crystal population in the andesite lava. As all of these growth rates are estimations, residence times should be taken with extreme caution and as estimated averages, specifically used for the relative comparisons of residence times between the compositions.

3.4.1. Basalts

To estimate the residence time of the basaltic lavas prior to eruption, a constant growth rate was chosen dependent on the nature of the plagioclase crystals (groundmass, microlites, etc.). CSD Slope, resident times, and growth rates (following Brugger and Hammer, 2010) used are shown in Fig. 6a and b and results are given in Table S3 (Supplementary material). For basaltic lavas, the majority of the crystals are microlites. Assuming that they formed syn-eruptively, a growth rate of x10^{-8} mm s^{-1} was selected (Brugger and Hammer, 2010). Based on Eq. 1, the plagioclase population residence time constrains the lavas residence time of up to 100 days prior to eruption. These are similar timescales to those reported in the Borgarhraun lava field (Þeistareykir Volcanic System, N. Iceland), in which the timescale of final magma ascent and crystallisation was in the order of 20–50 days, indicating that magmas can ascend from the base of the crust to surface in less than 2 months (Mutch et al., 2017). These timescales are consistent with the overall crystal sizes of the population, as a population of smaller crystal sizes are associated with shorter residence times.

3.4.2. Basaltic andesites

To constrain the time window for fractional crystallisation occurring in the parental basalt, the residence time of the plagioclase crystal population in a basaltic andesite (51% SiO_2) was used. Assuming one crystal population based on the straight CSD (Fig. 6c) and a plagioclase growth rate of ~10^{-10} mm s^{-1} for plagioclase phenocryst in basaltic melts (Cashman, 1993), a residence time of 5.4 years for the population and for extension, for the basaltic andesite magma can be estimated (Eq. 1).

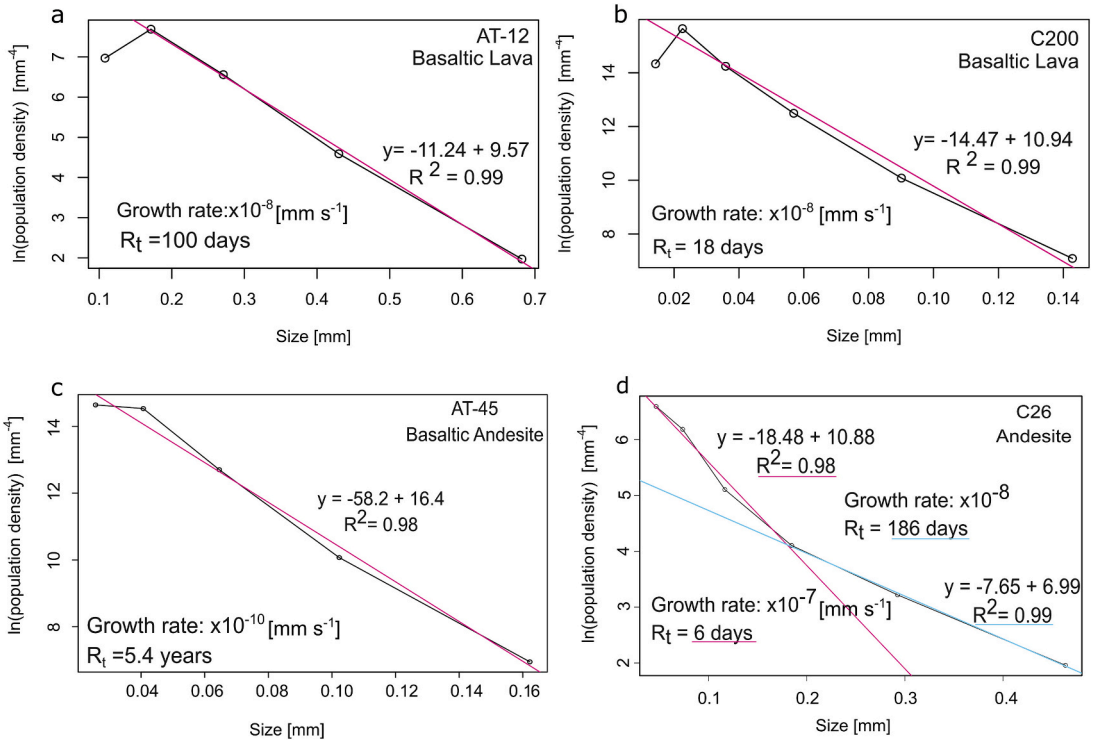

Fig. 6. Crystal size distribution (CSD) slopes for basaltic lavas (a and b), a basaltic andesite (c), and an andesite lava (d). Slope and R^2 values are given. Red lines show regression fit for population 1 crystals (a, b, c, d) and blue line shows regression fit for population 2 crystals (d only). Growth rate values in mm s^{-1}, and residence time (R_t) are shown for each CSD slope. (For interpretation of the references to colour in this figure legend, the reader is referred to the web version of this article.)

3.4.3. Andesites

For further crystallisation timescales, plagioclase in an andesite sample (C26) was chosen. The CSD shows two crystal populations (shown by the blue and pink lines in Fig. 6d)., Using a growth rate of $x10^{-7}$ mm s^{-1} (Brugger and Hammer, 2010) in eq. 1, a residence time of 186 days is estimated for one population, and 6 days for the other.

3.5. Isotopic data

In a diagram of $^{87}Sr/^{86}Sr$ vs $^{143}Nd/^{144}Nd$, isotope data (Table S4; Moscati and Hughes, 2024), Þingmúli lavas plot in the overlap between the MORB and OIB fields (Fig. 7a), and based on a $^{206}Pb/^{204}Pb$ vs $^{207}Pb/^{204}Pb$ diagram, Þingmúli lavas seem to have an affinity with the PREvalent MAntle (PREMA) reservoir (Fig. 7b). Although still within the PREMA field, the analyses show a strong affinity with an OIB mantle source (Fig. 7a). The HSR sample 0309–11, also appears to have

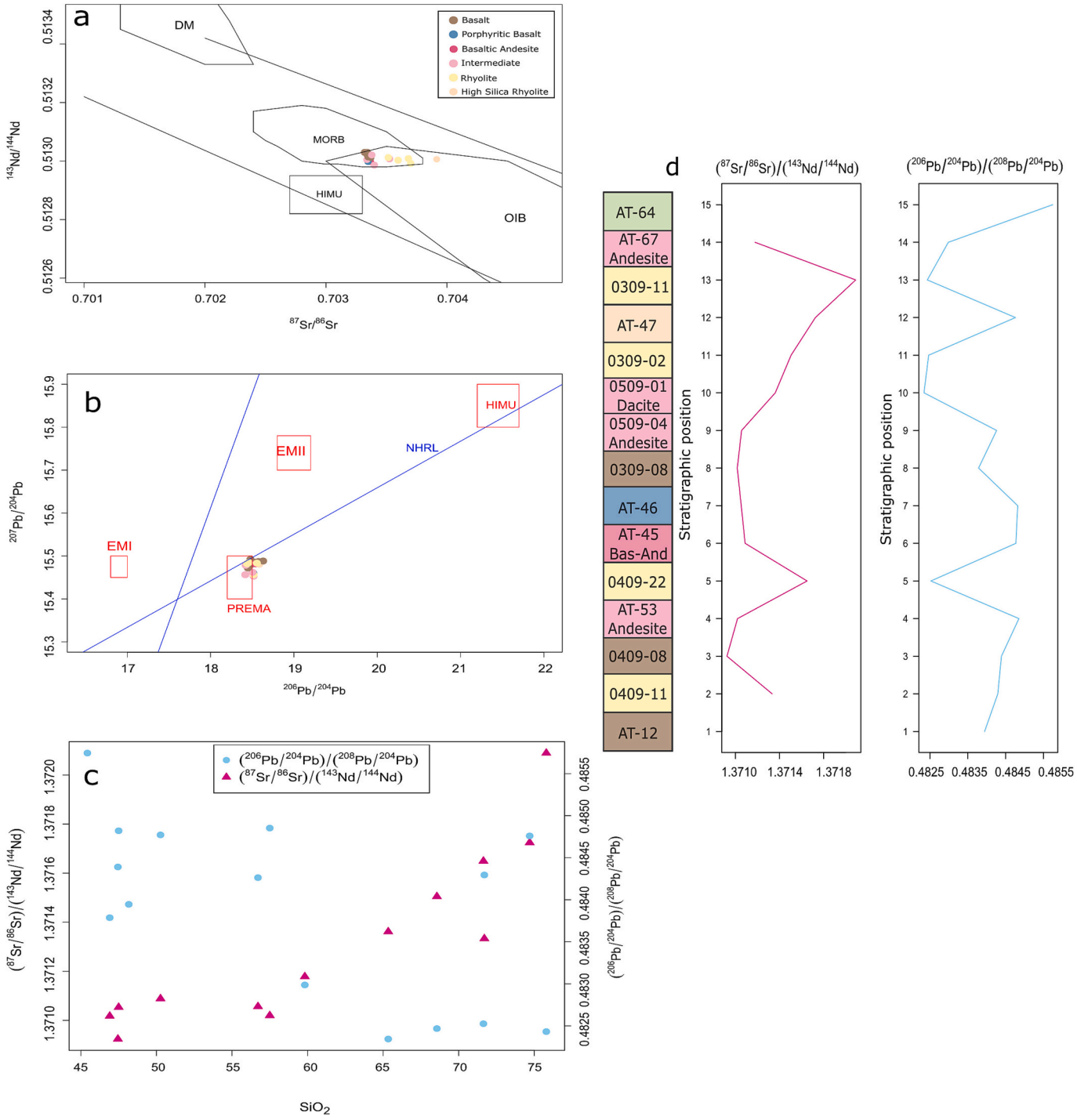

Fig. 7. Isotopic systematics of the Þingmúli lavas. a) $^{87}Sr/^{86}Sr$ versus $^{143}Nd/^{144}Nd$ with the mantle array (after Zindler and Hart, 1986). b) $^{206}Pb/^{204}Pb$ versus $^{207}Pb/^{204}Pb$ with mantle reservoirs (taken from Rollinson, 1993) to further determine magma sources. c) Changes in $(^{87}Sr/^{86}Sr)/(^{143}Nd/^{144}Nd)$ and $(^{206}Pb/^{204}Pb)/(^{208}Pb/^{204}Pb)$ against SiO_2. d) Changes in $(^{87}Sr/^{86}Sr)/(^{143}Nd/^{144}Nd)$ and $(^{206}Pb/^{204}Pb)/(^{208}Pb/^{204}Pb)$ over the stratigraphic order of analysed samples. Colours as in Fig. 1.

experienced an additional process since it has a higher $^{87}Sr/^{86}Sr$ than any other rhyolite lava (0.7039, compared to an average of 0.7036) at a similar $^{143}Nd/^{144}Nd$ ratio (Supplemental Fig. S1).

As the expected trends in an $^{87}Sr/^{86}Sr$ vs $^{143}Nd/^{144}Nd$ diagram and in the $^{206}Pb/^{204}Pb$ vs $^{207}Pb/^{204}Pb$ diagrams follow straight patterns (e.g., Hart, 1983) we have plotted their ratios (i.e., the slopes) vs SiO_2 in Fig. 7c. In an ideal fractional crystallisation model, the isotopic signatures should remain constant. However, Fig. 7c illustrates an increase in ($^{87}Sr/^{86}Sr$)/($^{143}Nd/^{144}Nd$) moving from basalt to rhyolite.

Basaltic andesites are more closely related to the basalts with similar ($^{87}Sr/^{86}Sr$)/($^{143}Nd/^{144}Nd$) and ($^{206}Pb/^{204}Pb$)/($^{208}Pb/^{204}Pb$) values. Andesite and dacite samples have more variable isotopic ratios (Fig. 4c), with higher ($^{87}Sr/^{86}Sr$)/($^{143}Nd/^{144}Nd$) ratios than the basalts, and with much lower ($^{206}Pb/^{204}Pb$)/($^{208}Pb/^{204}Pb$) ratios. Additional isotopic diagrams are given as Supplemental Figs. S1 and S2.

Examining the change in isotopic ratios over the volcanic stratigraphy (Fig. 7d) shows a marked difference between basalts and rhyolites, with the rhyolites toward the upper section of the stratigraphy (a HSR eruption) showing the highest enrichment in $^{87}Sr/^{86}Sr$ (highest ($^{87}Sr/^{86}Sr$)/($^{143}Nd/^{144}Nd$) ratio). The basaltic and basaltic andesite samples in the middle of the stratigraphy (stratigraphic positions 6–9) show the highest levels of depletion with higher $^{143}Nd/^{144}Nd$ (lowest ($^{87}Sr/^{86}Sr$)/($^{143}Nd/^{144}Nd$) ratio) indicating a more depleted, or less contaminated source than the rhyolites. The similar ratio suggests these samples are related. This is mirrored by similar ($^{206}Pb/^{204}Pb$)/($^{208}Pb/^{204}Pb$) ratios, with only a basalt (stratigraphic position 8 in Fig. 7d; 0309–08) showing a higher $^{208}Pb/^{204}Pb$ (lower ($^{206}Pb/^{204}Pb$)/($^{208}Pb/^{204}Pb$) ratio). Similarly, basalts and rhyolites (and the dacite sample, stratigraphic position 10; 0509–01) show notable differences in ($^{206}Pb/^{204}Pb$)/($^{208}Pb/^{204}Pb$) ratios, i.e., 0.4825, compared to 0.4845.

4. Discussion

4.1. Basaltic magmas

As shown in Figs. 2a-i and 3a-g, the basaltic lavas from Þingmúli can be described as transitional alkaline, with some more tholeiitic, and with trace element concentrations and isotopic ratios consistent with an OIB or PREMA source (Figs. 7a and 8a). In Iceland, transitional alkaline basalts have regularly been modelled as the results of partial melting within the Iceland plume (e.g., van der Meer et al., 2021; Viccaro et al., 2015; Jakobsson et al., 2008), specifically from the region outside of the centre (Jordan et al., 2022).

Assuming a lifespan for Þingmúli of between 1 and 2 Myr (based on lifespans of other East Fjords volcanoes, e.g., Breiðuvík and Kækjuskörð (Carley et al., 2017)) and a constant spreading rate of up to 2 cm year^{-1} (van Andel and Bowin, 1968), Þingmúli moved up to 40 km from the centre of the plume during its lifespan. Since the exact distance to the plume centre is variable, the degree of partial melting, and thus the composition of the basaltic magma produced, will vary. Partial melting in areas closer to the centre of the plume (where temperatures are higher) will result in a higher degree of partial melting, producing more tholeiitic magmas (i.e., depleted in incompatible elements; Harðardóttir et al., 2022). Partial melting further from the centre of the plume (where temperatures are lower) will produce more alkaline magmas. This distance factor may explain the occurrence of two types of basalts at Þingmúli, where some basalts are more tholeiitic than the most (Fig. 2a).

Initial estimations of mantle source compositions using rare earth elements (REE) show that the most likely source for the basalt lavas at Þingmúli is a spinel-bearing lherzolite (Fig. 8b). Partial melting is likely to be no more than 15–20% of the mantle source. Geochemical modelling of major elements (Fig. 9; Table S5: Supplementary material) was conducted using pMELTS (Ghiorso et al., 2002) to estimate the degree of partial melting of various mantle compositions to generate Þingmúli basalts.

The first step was determining the composition of the primary melts generated beneath Þingmúli. Assuming the basaltic lavas underwent some degree of fractional crystallisation prior to eruption, we first estimated the expected removed mineralogy using pMELTS, in a fractional crystallisaiton isobaric model, starting from sample AT-50 at 1.5 GPa. The aim of this step was to determine the removed mineralogy that would decrease the MgO content from primary melt values (e.g., ~8–10 wt%) to the average value in Þingmúli's erupted basalts (i.e., ~5–6 wt %). Under those conditions, the expected removed mineralogy is composed of 20 g of clinopyroxene and 3 g of olivine out of 100 g of basalt.

Then, using the Olive code (Cortés, 2016), we added the composition of the removed mineralogy to the composition of the basalts, in increment of 1 wt% until reaching a 10 wt% target MgO content. We also corrected the trace elements, based on a reverse Rayleigh fractionation model assuming the same given mineral extract, to calculate the bulk-rock partition coefficients of the relevant trace element (individual partition coefficients used in the calculation are from Rollinson, 1993). Corrected analyses are given in Table S6.

After this, seven lherzolites, with full geochemical data (Table 1), were selected from the GEOROC database (Lehnert et al., 2000 and references therein). Assuming a density of ~2.8 g/cm^3 of the rock column, and an estimation of the base of the Icelandic crust (approx. 40 km) in the East Fjords (Volk et al., 2021), the lithostatic pressure was constrained to 1–1.5 GPa. Assuming a reversible process, partial melting of these lherzolites was modelled as the reverse of an equilibrium crystallisation pMELTS calculation. In reality, reverse crystallisation overestimates melt fractions near the solidus, i.e., is a poor approximation at very low fractions but good at moderate-high melt fractions, therefore results need to be considered with caution (e.g., Ghiorso and Stolper, 1999). Major element modelling was complemented with batch melting trace element calculations using partition coefficients data from Rollinson (1993).

Assuming that the mantle at this depth is a spinel lherzolite, 15 to 20% of partial melting can most accurately reproduce the composition of Þingmúli basalts (Fig. 9), particularly, their Al_2O_3 and MgO concentrations (Fig. 9). However, the model cannot accurately reproduce the Na_2O and K_2O contents, suggesting an additional process such as contamination or post-eruption hydrothermal alteration. Furthermore, the partial melting models produce lower TiO_2 concentrations than those found in Þingmúli basalts. Processes such as contamination/assimilation of a high TiO_2 concentration crust (i.e., basaltic deposits from the Reyðarfjörður volcano, which have up to 4 wt% TiO_2) may explain this discrepancy.

To account for a wide variety of mantle heterogeneities, partial melting modelling of additional lherzolite samples L151 and L169 from the GEOROC database (Lehnert et al., 2000) was carried out to give a broad spectrum of potential trace element concentrations (Fig. 9). A harzburgite partial melting model (H112; Chen et al., 2017), was added for comparison. The batch melting of these lherzolite compositions can reproduce the lower concentrations of Sr and Ba found in the Þingmúli basalts.

Basaltic lavas with up to 350 ppm of Sr, will require a source more enriched in Sr or a smaller degree of partial melting. For example, sample JAG690–11 garnet lherzolite (Grégoire et al., 2002) containing ~49 ppm of Sr would produce a melt with ~410 ppm of Sr after 10% of partial batch melting. On average, the garnet lherzolites published in GEOROC contain ~43 ppm of Sr, but analyses with 100 ppm or more are also possible.

Other trace elements such as Th and Nb can all be reproduced by the lherzolite melting models, with some higher concentrations (i.e., Ta, which may be explained by the presence of magnetite and ilmenite in many of the basalt samples) requiring a more enriched source. Zr concentrations in all models are slightly lower than the target compositions (up to 400 ppm) in the basalts, and may reflect contamination with a high Zr source, e.g., an OIB type crust, or volcanic deposits from volcanoes fed by the mantle plume.

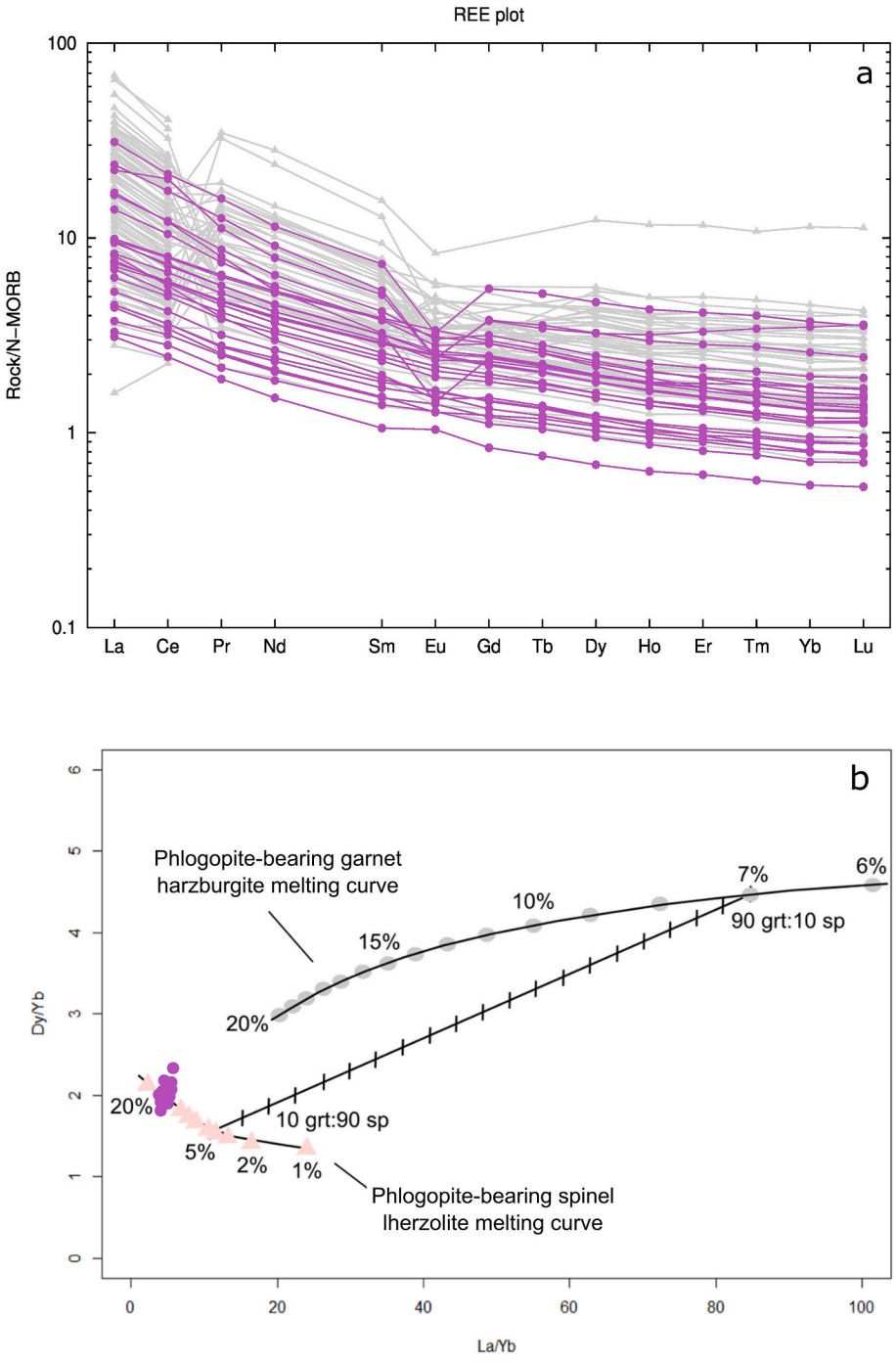

Fig. 8. a) Þingmúli basalts normalised against N-MORB (Sun and McDonough, 1989). b) An estimation of source compositions using non-modal batch partial melting models based on Dy/Yb vs. La/Yb. Partial melting curves from Qi et al. (2017); grt: Garnet, sp.: Spinel. Filled symbols illustrate degree of partial melting from start composition. Dy/Yb and La/Yb are normalised to chondrite values from Sun and McDonough (1989).

4.2. Rhyolitic magmas

Based again on the rhyolite-MELTS fractional crystallisation model starting from sample AT-50 (Supplemental Material Table S7b), the proportions of more evolved compositions produced from a basaltic magma should be of the order of 37–28 vol% of basaltic andesite, 27–21 vol% of andesite, 20–15 vol% of dacites and 14–13 vol% of rhyolites. Although not all of the potentially generated magmas would have erupted, is very likely that the decrease in volume between the basalts to intermediates and between the intermediates to the rhyolites is reflected in the eruptive deposits, along with geochemical characteristics which reflect a fractional crystallisation process (e.g., low concentrations of incompatible elements, and isotopic systematics similar to the parent basalt).

At Þingmúli, the volume of rhyolite (approx. 25 vol% of the total eruptive volume) vastly exceeds this estimation and more crucially, it exceeds the volume of erupted intermediates (Table S8), and their geochemical characteristics are not consistent with a fractional crystallisation model. For example, the concentrations of incompatible elements (which should increase during fractional crystallisation) are broadly similar to basaltic lavas (e.g., between 200 and 400 ppm of Zr; Fig. 3). Additionally, their isotopic systematics show differences

compared to the basaltic lavas (i.e., 0.703681 $^{87}Sr/^{86}Sr$ in rhyolite compared to 0.703371$^{87}Sr/^{86}Sr$ in basaltic lavas), which strongly suggests these are not derived from the basaltic lavas via fractional crystallisation.

Thus, we favour a partial melting mechanism, using potential starting compositions from the sequence of lava (basaltic-andesitic) and dacite-rhyolite pyroclastic layers beneath Þingmúli (Table 2) logged in detail by the Icelandic Research Drilling Project (e.g., Flower et al., 1982).

Plotting the normative mineralogy of the rhyolites onto the haplogranite system, including granitic melt minima at different pressures (Tuttle and Bowen, 1958), suggests that the depths at which partial

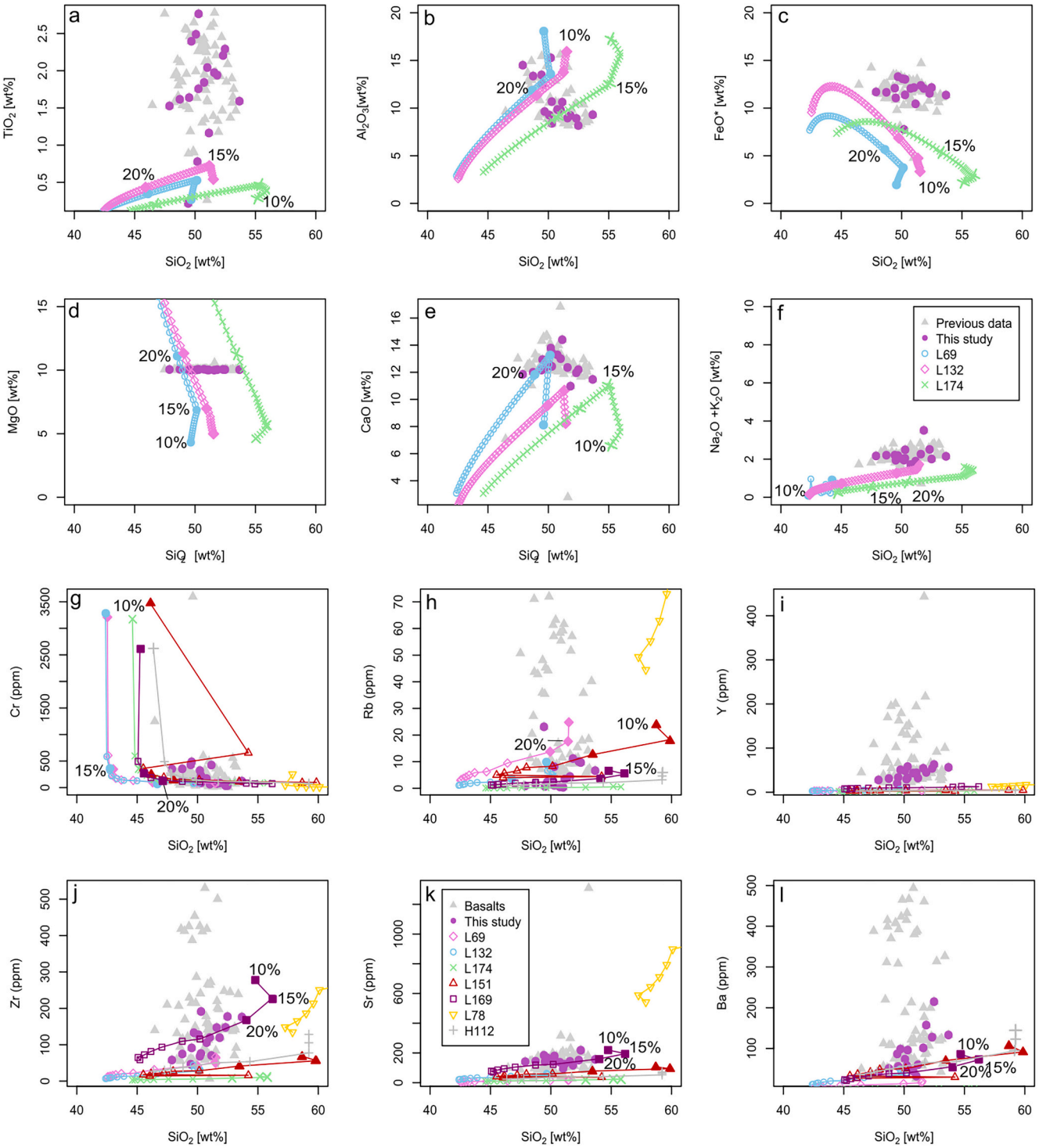

Fig. 9. a-f) Variation diagrams of major elements vs SiO_2, g-l) Variation diagrams of selected trace elements vs SiO_2, showing the geochemical modelling of lherzolite and harzburgite samples to produce corrected basaltic lavas by reversing fractional crystallisation at Þingmúli (see text for the detail). LXX denotes Lherzolite sample, HXX denotes Harzburgite sample. Each sample melting line is denoted by a colour, and Þingmúli basalts from this study are shown as filled purple circles and previous data from Charreteur et al., 2013; and Carmichael, 1962, 1964 are shown as grey triangles.Starting compositions, references and modelling parameters are given in Table 1. (For interpretation of the references to colour in this figure legend, the reader is referred to the web version of this article.)

Table 1
Starting compositions and input parameters for all mantle partial melt modelling used in this study. Run reference corresponds to those given in Fig. 9. LXX denotes Lherzolite sample, HXX denotes Harzburgite sample. All mantle composition samples taken from GEOROC, 2023 (Lehnert et al., 2000; L69; Vaselli et al., 1995, L132: Hsu et al., 2000, L174; Martin et al., 2015, L151; Hsu et al., 2000, L169; Brooker et al., 2004, L78; Rhodes and Dawson, 1975, H112; Chen et al., 2017). Starting compositions chosen based on the position of basalts in Fig. 8b, with harzburgite added for comparison.

Run Reference	L 39	L123	L174	H112	L151	L196	L78
GEOROC id	8226	12,085	19,201	20,886	12,085	13,123	17,870
Lithology	Lherzolite	Lherzolite	Lherzolite	Harzburgite	Lherzolite	Lherzolite	Lherzolite
Starting Intrinsic conditions (T,P, intrinsic fO_2)	2000–1000 °C, 1.5 GPa, QFM −1	2000–1000 °C, 1.5 GPa, QFM −1	2000–1000 °C, 1.5 GPa, QFM −1	2000–1000 °C, 1.5 GPa, QFM −1	2000–1000 °C, 1.5 GPa, QFM −1	2000–1000 °C, 1.5 GPa, QFM −1	2000–1000 °C, 1.5 GPa, QFM −1
Starting MELTS conditions	Isobaric, Equilibrium Crystallisation	Isobaric, Equilibrium Crystallisation	Isobaric, Equilibrium Crystallisation	Isobaric, Equilibrium Crystallisation	Isobaric, Equilibrium Crystallisation	Isobaric, Equilibrium Crystallisation	Isobaric, Equilibrium Crystallisation
Starting composition	42.3777	42.5313	44.6074	46.35	46.05	45.23	57.87
SiO_2 (wt%)	0.1161	0.1375	0.1192	0.11	0.25	0.26	0.75
TiO_2 (wt%)	2.9123	2.5931	3.2784	1.5	1.73	3.24	20.37
Al_2O_3 (wt%)	0.6548	0.7511	0.606	0.999	1.292	1.417	0.518
Fe_2O_3 (wt%)	7.6817	9.5698	7.358	5.092	6.588	7.225	2.644
FeO (wt%)	3.0768	0.1277	0.1292	0.2	1.72	2.71	7.79
MnO (wt%)	37.898	39.8399	38.5571	42.67	42.23	38.23	3.37
MgO (wt%)	3.0768	2.1708	3.0599	0.08	0.13	0.15	0.07
CaO (wt%)	0.2032	0.2259	0.2583	0.02	0.12	0.114	1.96
Na_2O (wt%)	0.0561	0.0491	0.0298	0.01	0.33	0.31	4.13
K_2O (wt%)	0.0116	0.0393	0.0099	0	0.06	0.03	0.5
P2O5 (wt%)	1.935	1.9645	1.9869	2.18	0	0.15	0
H_2O (wt%)	1.123	3	0.129	1.01	4	1.16	44.47
Rb (ppm)	20.6	5	8.2	23.41	34.5	71.27	541.3
Sr (ppm)	11.51	4	0.45	36.27	27	21.24	635.2
Ba (ppm)	2.61	201	1.676	2.85	2.75	7.17	12.33
Y (ppm)	7	11	2.864	27.21	14.5	58.8	134.3
Zr (ppm)	0.143	0.36	0.077	0.7	0.25	0.481	2.65
Hf (ppm)	0.921	1.2	0.128	4.12	2.3	8.83	51.7
Nb (ppm)	0.065	0.07	0.127	0.202	0.2	0.36	3.03
Ta (ppm)	0.122	0.07	0.019	0.089	0.6	0.17	4.39
Th (ppm)	0.099	0.02	0.009	0.102	0.06	0.06	1.32
U (ppm)	2023	2095	1865.3	2520.9	2003	1923	297.9
Ni (ppm)	95	108.8	121.3	98.13	98.1	65	25.3
Co (ppm)	64	55	68.6	72.74	42.5	70	110.8
V (ppm)	3293	3218	3176.9	2602.5	3484	2623	251.4
Cr (ppm)	15	9	13.5	11.36	8	13	19.6
Sc (ppm)							

Table 2
Starting compositions and input parameters for partial melting of lithologies beneath Þingmúli. Run reference corresponds to those given in Fig. 11. Lithology compositions from Flower et al. (1982). Starting pressure estimated using depths constrained in Fig. 10. Water content estimated from loss of ignition (LOI) values given in Flower et al. (1982).

Run Reference	804 m	656 m	1165 m
Starting Intrinsic conditions (T,P, intrinsic fO_2)	2000–650 °C, 100 MPa, QFM −1	2000–650 °C, 100 MPa, QFM −1	2000–650 °C, 100 MPa, QFM −1
Starting MELTS conditions	Isobaric, Equilibrium Crystallisation	Isobaric, Equilibrium Crystallisation	Isobaric, Equilibrium Crystallisation
Starting composition			
SiO_2 (wt%)	51.3145	52.8734	66.2346
TiO_2 (wt%)	3.1615	2.1968	1.6727
Al_2O_3 (wt%)	12.7994	15.1262	11.7329
Fe_2O_3 (wt%)	1.5037	1.3245	1.0582
FeO (wt%)	11.9484	9.8641	9.0307
MnO (wt%)	0.2006	0.1699	0.1083
MgO (wt%)	4.5183	3.609	1.6638
CaO (wt%)	9.3389	8.5713	2.4578
Na_2O (wt%)	2.7671	2.9266	4.4223
K_2O (wt%)	0.9429	1.8389	0.1382
H_2O (wt%)	1.5047	1.4992	1.4806
Zr (ppm)	263	334	288
Y (ppm)	55	51	45
Rb (ppm)	6	28	0
Nb (ppm)	35	39	27
Sr (ppm)	364	306	233

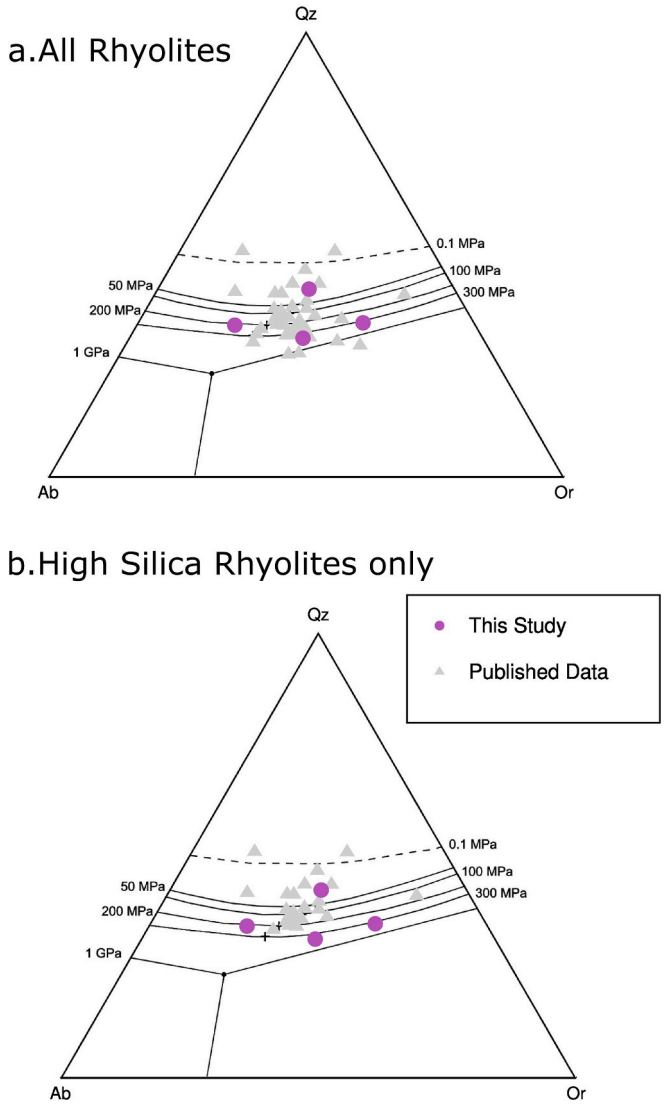

Fig. 10. a) Þingmúli rhyolites from this study and literature, plotted on the haplogranite minimum after Tuttle and Bowen (1958) based on their normative Quartz (Q), Orthoclase (Or) and Albite (Ab), corrected for Anorthite content (Blundy and Cashman, 2001). Lines denote cotectics at various pressures in MPa. b) Shows only the high silica rhyolites (HSR) found at Þingmúli, i.e., rhyolites with more than 75% of SiO2 on a dry basis.

melting took place were shallow, in the upper 2 km of the crust (100–50 MPa; Fig. 10a), with the HSR melts likely generated in the upper 0.5 to 1 km of the crust (less than 50 MPa; Fig. 10b). This is consistent with a more radiogenic $^{87}Sr/^{86}Sr$ signature as during ascent these melts would have interacted more with the surrounding crust. These depths are also consistent with other reported occurrences of shallow rhyolite generation in Iceland, e.g., HSR magma was intersected at depths of up to 2.1 km during drilling at Krafla (Zierenberg et al., 2013). As the rhyolitic compositions have been plotted using normative mineralogy calculated based on whole rock geochemistry and corrected following Blundy and Cashman (2001), depth estimation should be considered a minimum estimation.

Partial melting modelling was conducted using rhyolite-MELTS (Gualda et al., 2012; Asimow and Ghiorso, 1998; Ghiorso and Sack, 1995), again considering such process as a reversed equilibrium crystallisation thermodynamic process. Starting compositions were taken from known stratigraphy beneath Þingmúli (detailed during the Iceland Research Drilling Project; IRDP), thought to originate from the nearby Reyðarfjörður central volcano (Flower et al., 1982). Three layers were chosen as representative of the common lithologies found in the Reyðarfjörður Volcanic Sequence (RVS). Runs 1 and 3 are basaltic andesite lavas found at 804 m depth and 656 m depth respectively and Run 2 is a dacitic ignimbrite found at 1165 m depth.

Partial melting starting from basaltic andesites accurately reproduces Þingmúli rhyolites with SiO_2 ranging from 70 to 76 wt% and all major elements within 1 wt% from Þingmúli rhyolites analyses (Fig. 11 a and b). The modelling overestimates K_2O concentration (i.e., ~6 wt% compared with the ~3 wt% found in most Þingmúli rhyolites), which may be explained by a high K_2O starting concentration, likely due to hydrothermal alteration of these layers (Flower et al., 1982). Partial melting from the dacitic ignimbrite also fairly reproduces the Þingmúli rhyolites, with only K_2O underestimated, and is the only run to accurately reproduce the higher silica rhyolites. This different source for the HSR is consistent with the isotopic signatures, where HSR is distinct from other rhyolites with a higher concentration of $^{87}Sr/^{86}Sr$.

Partial melting processes can also be modelled using the trace element data (Fig. 11a-l), from Flower et al. (1982) for the RVS. Starting with known concentrations of Nb, Zr, Rb, Sr and Y in the underlying basalts and rhyolitic ignimbrites, a batch partial melting model reproduce the concentration of these elements in Þingmúli rhyolites (grey triangles and purple circles). In elements such as Rb, Y and Nb (Figs. 11j, j, and l) the upper, lower, and middle concentrations can be reproduced, with partial melting proportion up to 15%. There is some variation with the model failing to reproduce concentrations ~100 ppm Nb. This discrepancy may be explained by the occurrence of refractory titanite in the rhyolitic lavas (Carmichael, 1964), which typically concentrate this element.

Both batch and Raleigh partial melting models starting from basaltic-basaltic andesite Þingmúli compositions produce rhyolites with higher Sr concentrations (300–400 ppm) than Þingmúli rhyolites (<200 ppm; Fig. 11i). This may be explained by the crystallisation and removal of the assemblage albitic plagioclase + K-Feldspar and Quartz from the rhyolites as their compositions are close to a cotectic with either minimum or a eutectic point (Fig. 10), or from variations in the starting mineralogy of the source rock. It can be easily shown with a mass balance calculation that the removal of such assemblage will not change the major elements proportion while it will have a major influence in the trace element concentrations.

Modelled Zr concentrations by batch partial melting starting from the same initial compositions produce concentrations that are 600 ppm higher than in Þingmúli rhyolites (Fig. 11h). Models starting with the ignimbrite layers Zr concentration are able to reproduce the upper Zr content (i.e., 400 ppm and above), albeit with high degrees of partial melting (over 20%; Fig. 11h). This is due to a high Zr concentration in the Reyðarfjörður layers, which is noted to be high due to the 'high concentration of zircon crystals, presumably the result of sorting during fallout' (Schmincke et al., 1982). Thus, a batch partial melting model predicts concentrations up to 1000 ppm of Zr in Þingmúli rhyolite melts as this element is highly incompatible. However, as zircon is a well-known refractory mineral (e.g., Suzuki et al., 2005), the crystals are not easily melted during the host rock partial melting. Zirconium is in practical terms "locked" in the mineral phase, and it is not released into the resulting melt. This idea is supported by the $ZrO_2 - SiO_2$ phase diagram in which the zircon melting point at atmospheric pressure is at 1687 °C (Butterman and Foster, 1967; Timms et al., 2017). In a basaltic magma (the source of heat to promote partial melting in this case), the average temperature is between 1200 and 1400 °C with the higher temperatures in hotspot settings (e.g., Lee et al., 2009), which is not high enough to melt the zircon crystals occurring in the ignimbrite layer. It is also noted in Charreteur et al. (2013) that zircon crystals occur as inclusions within plagioclase phenocrysts, suggesting that zircons are carried as xenocrysts in the newly formed rhyolite magma.

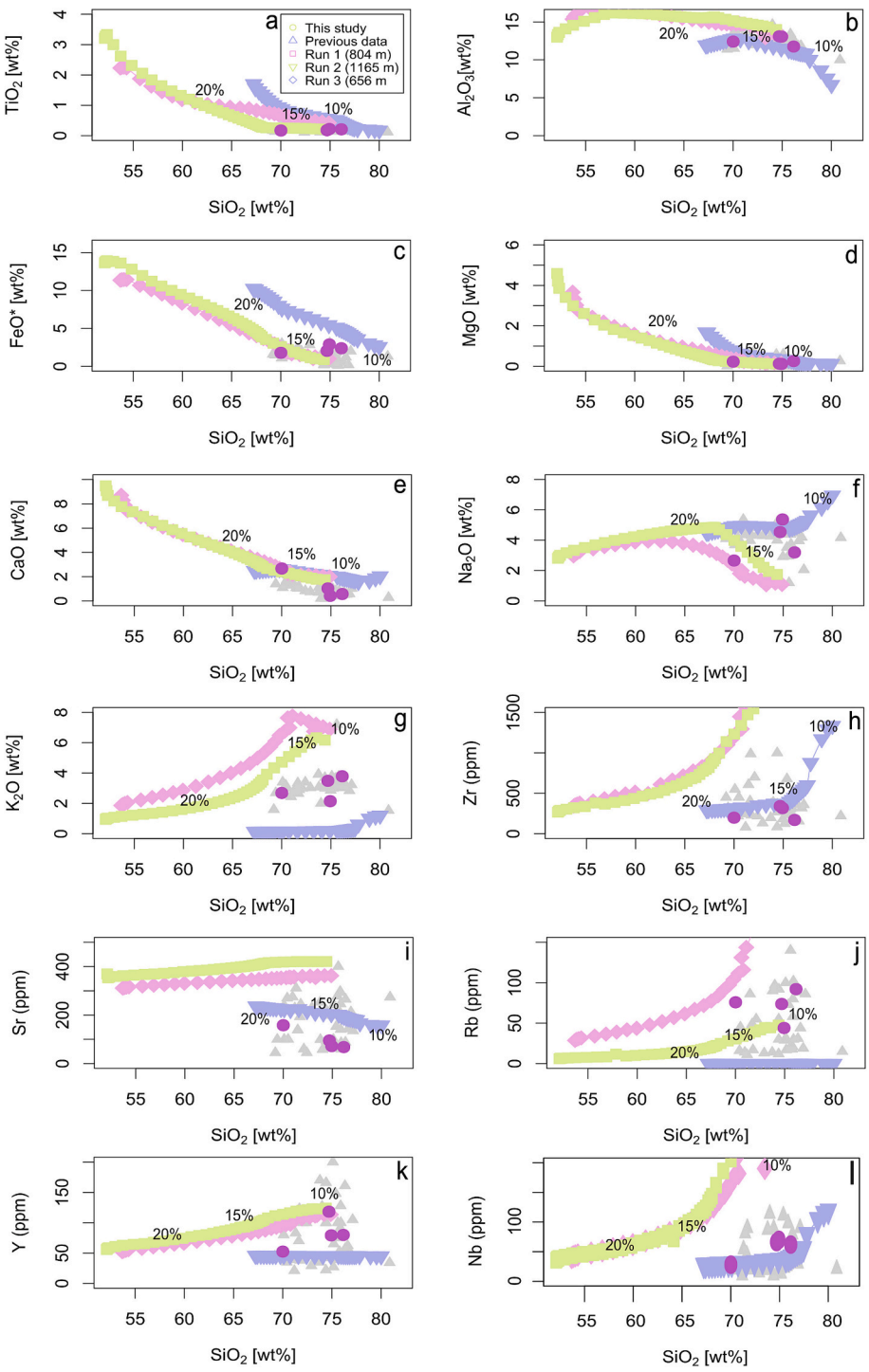

Fig. 11. Partial melting modelling producing the rhyolitic lavas. Grey triangles show Þingmúli rhyolites (Charreteur et al., 2013; Carmichael,1962) and purple circles show rhyolites from this study. Each partial melting model (green, pink, and purple lines) corresponds to the depth of a given layer identified by Helgason and Zentilli (1982) and Flower et al. (1982). Runs 1 and 3 (green and pink) are basaltic-andesite lavas at 804 and 656 m and run 2 (purple) is a dacitic ignimbrite at 1165 m from the Reyðarfjörður Volcanic Sequence below Þingmúli. a-g) show major elements vs SiO_2. h-l) show trace element variation with SiO_2. Colours and symbols same in all diagrams. Starting compositions and modelling parameters given in supplementary material. (For interpretation of the references to colour in this figure legend, the reader is referred to the web version of this article.)

4.3. Basaltic andesite, andesite and dacite magmas

Basaltic andesites, andesites and dacites at Þingmúli are comparatively scarce, forming only 9 vol% of all lavas erupted. Their scarcity suggests that the magma processes that produced them did not operate continuously during Þingmúli's lifespan. If produced by fractional crystallisation, these magmas should contain relatively higher concentrations of incompatible elements, a similar isotopic signature to the parent basalt, and on average, mineral chemistries suggesting an evolving magma. In addition, residence times should be longer than in a basaltic magma, reflecting the time spent evolving in the plumbing system prior to eruption.

However, it is only the basaltic andesites that appear consistent with a fractional crystallisation trend. Andesites and dacites as shown in Fig. 3a-f have broadly similar incompatible element concentrations as the basaltic lavas i.e., between 0 and 50 ppm Rb (Fig. 3e) and no significant decrease in Sr (between 200 and 300 ppm) as would be expected if plagioclase was fractionating from the magma (Fig. 3c). It is worth noting here the noisy spread of the literature data, adding some uncertainty to our conclusions. Regardless, the petrography highlights disequilibrium between the crystal cargos (i.e., sieve textures found in plagioclases) and their melt compositions (Fig. 4e), while mineral chemistry, reflects crystal growth in a more primitive magma (Fig. 5b), with disequilibrium reported between plagioclase core and rims (Section 3.3.2). Calculated residence times estimated from the CSD of their main mineral phases also suggest these magmas spend a relatively shorter time in the plumbing system, cooling and evolving than basaltic magmas, the opposite of what is expected if they were produced by fractional crystallisation.

An alternative mechanism to generate the andesite and dacite melts is by mixing basaltic and rhyolitic melts. To test this mechanism, we have plotted major and trace elements on an abacus diagram (McGarvie et al., 1990; Fig. 12), using representative basaltic and rhyolitic lava analyses (T1–04 and 0409–09, respectively) as mixing endmembers (further mixing models can be found in Supplemental Fig. S3). The andesite lavas (AT-25, 0509–04, T6–03) all plot as roughly vertical lines, with only AT-25 and 0509–04 having variation in Sr, suggesting additional plagioclase fractionation after mixing. Based on Fig. 12, andesite and dacite magmas can be generated from 80:20 to 60:40 (basalt: rhyolite) depending on the SiO_2 content desired. The dacitic lava (sample 0309–02) plots as a roughly vertical line, with only variation in Zr, which can be improved using a lower Zr concentration rhyolite as the mixing endmember, requiring a larger contribution of rhyolite, between 20:80 to 10:90 (basalt:rhyolite).

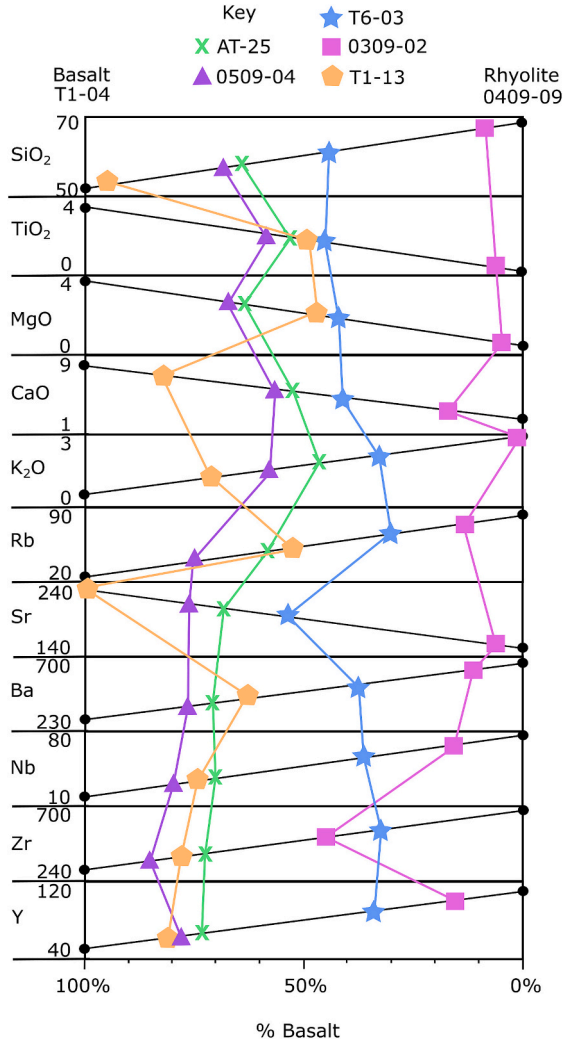

Fig. 12. Abacus diagram illustrating mixing between a rhyolite and basalt. The x-axis shows the proportion of the basaltic endmember. The y axis gives major elements (wt%) and trace element (ppm) concentrations. Black circles represent the composition of that element or oxide in the endmember magmas. Samples AT-25, 0509–04 and T6–03 are andesitic lavas, 0309–02 is a dacite lava and T1–13 is a basaltic andesite lava. All samples, apart from AT-25, are taken from Charreteur (2012).

4.4. *Basaltic andesite magmas*

However, this mixing model does not easily reproduce basaltic andesites, (sample T1–13; Fig. 12), in which TiO_2 and MgO are in lower concentration than would be expected, while Rb, Ba, Zr, Y and Nb are higher. Petrography of the samples also corroborates an absence of clear mixing textures (i.e., lack of sieve textures or reverse zoning). Additionally, the basaltic andesite samples seem to have only one plagioclase crystal population with relatively longer residence times than the andesitic samples based on their CSDs. Based on all this evidence, we propose a fractional crystallisation mechanism from a parental basalt magma.

A fractional crystallisation model such as the MELTS model starting from sample AT-50 (Figs. 2a - i) generating the basaltic andesites would also explain the curved trend in the high FeO, TiO_2 basalts, where enrichment in these elements is observed up to 54 wt% SiO_2 (Fig. 2b and d). The mechanism would also explain the concentrations of incompatible elements such as Zr in the basaltic andesites (Fig. 3a) compared to other evolved compositions.

5. Comparisons with other active central volcanoes

Whole-rock chemistry of Þingmúli's eruptive products is consistent with an enriched source, with basaltic samples being broadly transitional alkaline, implying that Þingmúli was likely a flank zone volcano, which formed, and erupted adjacent to the tertiary rift zone. Based on the assumption that the Icelandic plume has moved marginally over the last 10 Ma (Thordarson and Höskuldsson, 2022), Þingmúli would have been situated approx. 90 km from the centre of the plume when it was active. The tectonic environment of the East Fjords at this time would have been similar to the current Öræfi volcanic belt (ÖVB), a flank zone volcanic region located approx. 50 km adjacent of the central rift zone (Thordarson and Larsen, 2007).

In a geochemical comparison with Öræfajökull, the basalts at Þingmúli display a similar compositional range in alkalis, plotting in the transitional alkali zone (Supplemental Fig. S4a). Charreteur et al. (2013) made a similar comparison, identifying similarities in FeO* trends between both central volcanoes, and postulated that trends between a low- and a high-iron trends can be generated via mixing of these two endmembers. Both volcanoes exhibit a broadly similar concentrations of Zr in their basalts (clustering around 200–400 ppm) representing their enriched mantle source origin, however a wider range is observed at Þingmúli, with some basalts containing up to 500 ppm Zr, and a small cluster at ~700 ppm. This may illustrate either a wider range of partial melting amounts at Þingmúli, compared to Öræfajökull, or a difference in source composition (mantle heterogeneities). The generation of intermediate magmas (andesite and dacite) at Öræfajökull is thought to be the result of magma mixing between basalt and rhyolite, with the rhyolite itself generated via partial melting of older crust (Prestvik et al., 2001; Selbekk and Trønnes, 2007).

In comparison to other modern day central volcanoes (both rift and flank zone), Þingmúli also bears geochemical resemblance to Hekla, which currently sits approx. 120 km from the centre of the plume. Both

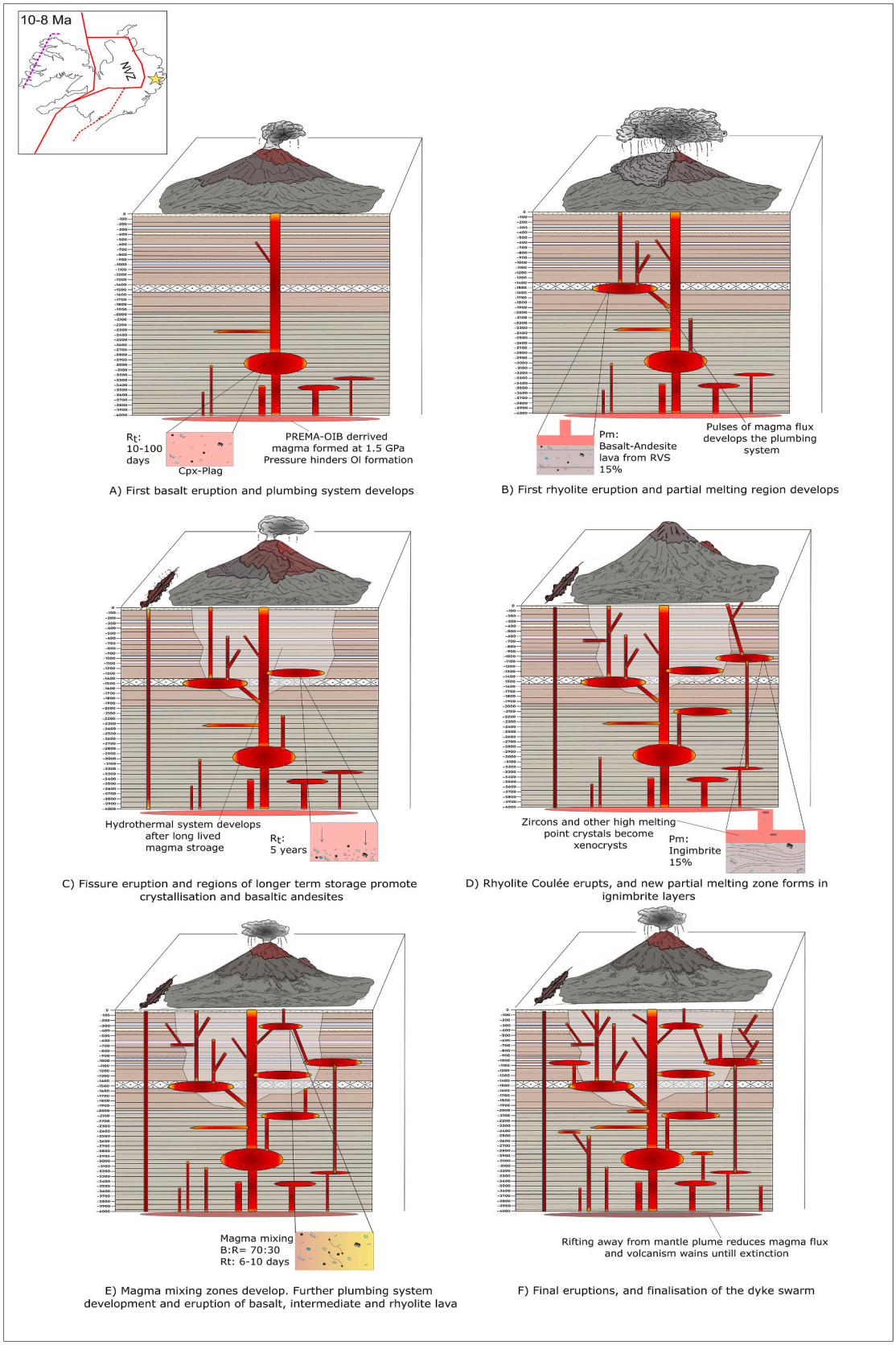

(caption on next page)

Fig. 13. The petrogenetic and volcanic evolution of Þingmúli. Stage one (a) involves the first magmas sourced from the mantle plume at 1.5 GPa erupting after 10–100 days in the plumbing system. The first magma storage zone also forms here. Stage 2 (b) is the first partial melting creating a large rhyolitic eruption. Continued magma flux continues to develop the plumbing system. Stage 3 (c) includes the formations of regions for crystallisation to create basaltic andesite magmas, on a timescale of 5 years. Long-lived magma storage and thermal input also lead to the formation of a hydrothermal system (Carmichael, 1962), and intrusions to the west creates a fissure eruption. Stage 4 (d) is the eruption of the rhyolite coulée from a newly formed partial melting zone. This is sourced from ignimbrite layers, the melting of which entrains zircons and other high-temperature minerals. Stage 5 (e) includes the development of areas of magma mixing, which produces both andesite and dacite magmas, which remain in the plumbing system for a timescale of days prior to eruption. Continued magma flux grows the hydrothermal system, and the plumbing system becomes more complex. Stage 6 (f) is the continued growth of the plumbing system, hydrothermal system and eruption of all lava types. This continues until the magma source is lost as Þingmúli rifts further from the mantle plume. Figure is not to scale, but depths (given in metres) are indicated to highlight the stratigraphy under Þingmúli, in particular, the depth of pyroclastic deposits (in yellow) and intermediate lavas (in pink) according to the Iceland Research Drilling Project at Reyðarfjörður (Flower et al., 1982). Top left inset shows a reconstruction of Iceland between 8 and 10 Ma, i.e., at the time Þingmúli was active. Red lines indicate active spreading margins; red dashed lines indicate emerging spreading margins and purple dashed line indicates extinct spreading margin. Þingmúli is denoted by the star; modified from Foulger (2003). (For interpretation of the references to colour in this figure legend, the reader is referred to the web version of this article.)

Þingmúli and Hekla show a broadly similar transitional alkaline trend (Supplementary Fig. S4a), and similarities between Zr concentrations, of around 400 ppm (Supplementary Fig. S4b). Hekla is well known to produce high volumes of intermediate lavas by magma mixing (e.g., Sverrisdottir, 2007), similar to what is proposed here for Þingmúli. Basaltic andesites are also a common occurrence at Hekla and, again similarly to Þingmúli, are thought to be the product of fractional crystallisation (e.g., Chekol et al., 2011).

6. Petrogenetic model

In summary (Fig. 13), basalts at Þingmúli are likely to be generated in the mantle as the result of partial melting in the outer region of the Icelandic plume. Toward the centre of the plume, higher temperatures would promote higher degrees of partial melting, thus generating more tholeiitic-trending basalts (Jakobsson et al., 2008; Jordan et al., 2022). Magmas generated at the outskirts of the Icelandic plume, will be generated by lower degrees of partial melting, producing transitional alkali basalts melts, slightly more enriched in incompatible elements and alkalis than the tholeiites. The ideal starting compositions to produce these basalts are spinel lherzolites undergoing 15–20% partial melting, at depths approx. 40–45 km (Fig. 13a), equivalent to the base of the Moho.

After their generation, the basaltic melt ascended, spending around a year in Þingmúli's plumbing system based on our residence time calculations. During this time, minor crustal contamination (likely basaltic crust) occurred and, in cases of melts with longer residence times, magmas likely underwent minor amounts of fractional crystallisation, producing basaltic-andesitic and/or ferro basalt magmas in approximately 5 years (Fig. 13b-c).

Rhyolites at Þingmúli are likely to have been generated by partial melting of the Reyðarfjörður Volcanic Sequence (RVS) beneath the volcano. Those with 70–75 wt% SiO_2 were the product of partial melting of basalt to basaltic andesitic lavas from the RVS as both rhyolite lava and pyroclastic eruptions (Fig. 13b). High silica rhyolites, with SiO_2 75 wt% and above, were generated by partial melting of dacitic ignimbrites and tuff layers from the RVS. They then erupted as a coulée on the eastern flanks of the volcano (Fig. 13d; Hughes, 2025).

Partial melting primarily occurred in the upper 1 km of the crust, with HSR requiring shallower depths (Gualda and Ghiorso, 2013). Andesite and dacite magmas at Þingmúli were produced by the shallow level mixing of basalt and rhyolite endmembers (Fig. 13e) with an average ratio of 60:30 basalt:rhyolite (up to 70:30 in cases of andesite production or mixing with high silica rhyolite to produce dacites). This mixing happened periodically across the whole of Þingmúli's lifespan, producing small, intermittent, lava flows fed by similar composition dykes, likely stemming from shallow level magma storage zone beneath the complex.

7. Conclusions

In this work, we have shown that the volcanic sequence at Þingmúli, originally interpreted as a tholeiitic sequence formed by fractional crystallisation, is really the consequence of combined fractional crystallisation, partial melting and magma mixing mechanisms starting from basalts generated in an enriched rather than a depleted mantle source.

Although a relative increase in FeO* does occur from basalts to basaltic andesites as expected in the tholeiitic differentiation, the majority of the eruptive products are in fact transitional alkaline. Of these, the evolved compositions are better modelled by partial melting of dacite-rhyolite pyroclastic layers beneath Þingmúli, while andesite and dacite compositions are the products of magma mixing between basalts and rhyolites (e.g., Reubi and Blundy, 2009).

This study highlights the importance of re-evaluating classic localities to refine our knowledge of magmatic processes and their implications on wider areas. In this case, Þingmúli, previously used as a case study for fractional crystallisation in Iceland, can now be used as a case study for magma mixing and partial melting for other Icelandic volcanoes with large volumes of rhyolite eruptions and comparatively smaller volumes of andesite and dacite magmas.

Supplementary data to this article can be found online at https://doi.org/10.1016/j.jvolgeores.2026.108561.

Credit authorship contribution statement

Amanda L. Hughes: Writing – review & editing, Writing – original draft, Methodology, Investigation, Formal analysis, Conceptualization. **Joaquín A. Cortés:** Writing – review & editing, Writing – original draft, Supervision, Methodology, Funding acquisition, Formal analysis, Conceptualization. **Dave McGarvie:** Writing – review & editing, Supervision, Methodology. **Richard J. Moscati:** Writing – review & editing, Methodology, Formal analysis. **Valerie Olive:** Methodology, Formal analysis.

Declaration of competing interest

Amanda Hughes reports financial support was provided by The Geological Society of London. If there are other authors, they declare that they have no known competing financial interests or personal relationships that could have appeared to influence the work reported in this paper.

Acknowledgements

We first acknowledge Stephen Mattox (Grand Valley State University), Margaret Hartley (University of Manchester), Kevin Jones (USGS), and an anonymous reviewer for a thorough review and suggestions, which greatly have improved the manuscript. AH would like to acknowledge her appreciation of Edge Hill University for project funding, and the Geological Society of London for granting funding to

contribute to sample collection and fieldwork. AH would also like to thank Robert Lowther from the Imperial College London for lending the thin section collection from I.S.E. Carmichael's, 1962 study to be re-studied. Any use of trade, product, or firm names in this publication is for descriptive purposes only and does not imply endorsement by the U. S. Government.

Data availability

Data will be made available on request.

References

Asimow, P.D., Ghiorso, M.S., 1998. Algorithmic modifications extending MELTS to calculate subsolidus phase relations. Am. Mineral. 83, 1127–1131.
Askew, R.A., 2020. Breiðdalur Central Volcano. What Came First: The Central Volcano or the Fissure Swarm? PhD thesis; University of Iceland.
Blundy, J., Cashman, K., 2001. Ascent-driven crystallisation of dacite magmas at Mount St Helens, 1980-1986. Contrib. Mineral. Petrol. 140, 631–650. https://doi.org/10.1007/s004100000219.
Brooker, R.A., James, R.H., Blundy, J.D., 2004. Trace elements and Li isotope systematics in Zabargad peridotites: evidence of ancient subduction processes in the Red Sea mantle. Chem. Geol. 212 (1–2), 179–204.
Brugger, C.R., Hammer, J.E., 2010. Crystal size distribution analysis of plagioclase in experimentally decompressed hydrous rhyodacite magma. Earth Planet. Sci. Lett. 300 (3–4), 246–254.
Bunsen, R.W., 1851. Uber die Processe der vulkanischen Gesteinsbildungen Islands. Ann. Phys. Chem. (Dritte Reihe). 83, 197–272.
Butterman, W.C., Foster, W.R., 1967. Zircon stability and the ZrO_2-SiO_2 phase diagram. Am. Mineral. 52, 880–885.
Carley, T.L., Miller, C.F., Sigmarsson, O., Coble, M.A., Fisher, C.M., Hanchar, J.M., Schmitt, A.K., Economos, R.C., 2017. Detrital zircon resolve longevity and evolution of silicic magmatism in extinct volcanic centers: A case study from the East Fjords of Iceland. Geosphere 13 (5), 1640–1663.
Carmichael, I.S.E., 1962. Volcanic Geology of Thingmúli: Eastern Iceland. PhD thesis. Imperial college, London.
Carmichael, I.S.E., 1964. The Petrology of Thingmúli, a Tertiary volcano in Eastern Iceland. J. Petrol. 5, 435–460.
Carmichael, I.S.E., 1967. The Mineralogy of Thingmúli, a Tertiary volcano in Eastern Iceland. Am. Mineral. 52, 1815–1841.
Carmichael, I.S.E., Turner, F.J., Verhoogen, J., 1974. Igneous Petrology. McGraw-Hill, New York, p. 739.
Cashman, K.V., 1993. Relationship between plagioclase crystallization and cooling rate in basaltic melts. Contrib. Mineral. Petrol. 113, 126–142.
Charreteur, G., 2012. Intermediate and Silicic Rocks in Accretion Context, Studies of the Thingmúli Volcanic System and of the Rauðafell Composite Complex Eastern Iceland. PhD thesis:. University of Aarhus.
Charreteur, G., Tegner, C., Haase, K., 2013. Multiple ways of producing intermediate and silicic rocks within Thingmúli and other Icelandic volcanoes. Contrib. Mineral. Petrol. 166, 471–490.
Chekol, T.A., Kobayashi, K., Yokoyama, T., Sakaguchi, C., Nakamura, E., 2011. Timescales of magma differentiation from basalt to andesite beneath Hekla Volcano, Iceland: Constraints from U-series disequilibria in lavas from the last quarter-millennium flows. Geochim. Cosmochim. Acta 75 (1), 256–283.
Chen, Y., Su, B., Chu, Z., 2017. Modification of an ancient subcontinental lithospheric mantle by continental subduction: Insight from the Maowu garnet peridotites in the Dabie UHP belt, eastern China. Lithos 278, 54–71.
Cortés, J.A., 2016. Olive, a simple fractional crystallisation calculator. Accessed in December 2025 from. https://theghub.org/resources/olive.
Cottrell, E., Birner, S.K., Brounce, M., Davis, F.A., Waters, L.E., Kelley, K.A., 2021. Oxygen fugacity across tectonic settings. In: Moretti, R., Neuville, D.R. (Eds.), Magma Redox Geochemistry. American Geophysical Union, pp. 33–61.
Einarsson, P., Sæmundsson, K., 1987. Earthquake epicenters 1982-1985 and volcanic systems in Iceland: A map. In: Sigfússon, Menningarsjóður (Ed.), Í hlutarins eðli, Festschrift for Þorbjörn Sigurgeirsson. Reykjavík.
Flower, M.F.J., Pritchard, R.G., Brem, G., Cann, J.R., Delaney, J., Emmerman, R., Gibson, I.L., Oakley, P.J., Robinson, P.T., Schmincke, H.U., 1982. Chemical stratigraphy, Iceland Research Drilling Project, Reydarfjordur, eastern Iceland. J. Geophys. Res. Solid Earth 87 (B8), 6489–6510.
Foulger, G.R., 2003. On the apparent eastward migration of the spreading ridge in Iceland. In: In *Proceedings of the Plume: VI.* Plume Hypothesis Conference, Geological Society of America, Hveragerdi, Iceland, Beyond the.
Franceschelli, M., Puxeddu, M., Cruciani, G., Dini, A., Loi, M., 2005. Layered amphibolite sequence in NE Sardinia, Italy: remnant of a pre-Variscan mafic silicic layered intrusion? Contrib. Mineral. Petrol. 149, 164–180.
Frost, C.D., Frost, B.R., 2022. Petrologic constraints on the origin of Proterozoic ferroan granites of the Laurentian margin. In: Whitmeyer, S.J., Williams, M.L., Kellett, D.A., Tikoff, B. (Eds.), Laurentia: Turning Points in the Evolution of a Continent, 220. Geological Society of America Memoirs. https://doi.org/10.1130/2022.1220(10.
Ghiorso, M.S., Sack, R.O., 1995. Chemical Mass transfer in Magmatic processes. IV. A revised and internally consistent thermodynamic model for the interpolation and extrapolation of liquidsolid equilibria in magmatic systems at elevated temperatures. Contrib. Mineral. Petrol. 119, 197–212.
Ghiorso, M.S., Stolper, E.M., 1999. Calculation of peridotite partial melting from thermodynamic models of minerals and melts. II. Isobaric variations in melts near the solidus and owing to variable source composition. J. Petrol. 40 (2), 297–313. https://doi.org/10.1093/petroj/40.2.297.
Ghiorso, M.S., Hirschmann, M.M., Reiners, P.W., Kress, V.C., 2002. The pMELTS: A revision of MELTS aimed at improving calculation of phase relations and major element partitioning involved in partial melting of the mantle at pressures up to 3 GPa. Geochem. Geophys. Geosyst. 3 (5). https://doi.org/10.1029/2001GC000217.
Gualda, G.A.R., Ghiorso, M.S., Lemons, R.V., Carley, T.L., 2012. A modified calibration of MELTS optimised for silica-rich, fluid bearing magmatic systems. J. Petrol. 53, 875–890.
Grégoire, M., Bell, D., Le Roex, A., 2002. Trace element geochemistry of phlogopite-rich mafic mantle xenoliths: their classification and their relationship to phlogopite-bearing peridotites and kimberlites revisited. Contrib. Mineral. Petrol. 142, 603–625.
Gualda, G.A., Ghiorso, M.S., 2013. Low-pressure origin of high-silica rhyolites and granites. J. Geol. 121 (5), 537–545.
Harðardóttir, S., Matthews, S., Halldorsson, S.A., Jackson, M.G., 2022. Spatial distribution and geochemical characterization of Icelandic mantle endmembers: Implications for plume geometry and melting processes. Chem. Geol. 604, 120930.
Hart, S.R., 1983. A large-scale isotope anomaly in the Southern Hemisphere mantle. Nature 309, 753–757.
Helgason, J., Zentilli, M., 1982. Stratigraphy and correlation of the region surrounding the IRDP drill hole 1978, Reydarfjordur, eastern Iceland. J. Geophys. Res. Solid Earth 87 (B8), 6405–6417.
Higgins, M.D., 2000. Measurement of Crystal size Distributions. Am. Mineral. 85 (9), 1105–1116.
Hsu, C.N., Chen, J.C., Ho, K.S., 2000. Geochemistry of Cenozoic volcanic rocks from Kirin Province, Northeast China. Geochem. J. 34 (1), 33–58.
Hughes, C.J., 1982. Igneous Petrology. Elsevier, New York, p. 551.
Hughes, A., 2025. The Magmatic Evolution of Þingmúli Central Volcano: Insights into Magma Evolution and Petrogenesis in Iceland. PhD Thesis,. Edge Hill University, Ormskirk.
Irvine, T.N., Baragar, W.R.A., 1971. A Guide to the Chemical Classification of the Common Volcanic Rocks. Can. J. Earth Sci. 8 (5), 523–548. https://doi.org/10.1139/e71-055.
Jakobsson, S.P., Jónasson, K., Sigurdsson, I.A., 2008. The three igneous rock series of Iceland. Jökull 58 (1), 117–138.
Jordan, M., Pilet, S., Brenna, M., 2022. Off-rift Axis Channelized Melt and Lithospheric Metasomatism along Mid-ocean Ridges—A Case Study from Iceland on the Limits of Melt Channelling. J. Petrol. 63 (7). https://doi.org/10.1093/petrology/egac052.
Lacasse, C., Sigurdsson, H., Carey, S.N., Jóhannesson, H., Thomas, L.E., Rogers, N.W., 2007. Bimodal volcanism at the Katla subglacial caldera, Iceland: insight into the geochemistry and petrogenesis of rhyolitic magmas. Bull. Volcanol. 69, 373–399. https://doi.org/10.1007/s00445-006-0082-5.
Lawver, L.A., Müller, R.D., 1994. Iceland hotspot track. Geology 22, 311–314.
Le Maitre, R.W., Dubek, A., Keller, J., Lameyre, J., Le Bas, M.J., Sabine, P.A., Schmid, R., Sorensen, H., Streckeisen, A., Woolley, A.R., Zanettin, B., 1989. A Classification of Igneous Rocks and Glossary of Terms: Recommendations of the International Union of Geological Sciences sub Commission on the Systematics of Igneous Rocks. Blackwell, Oxford, 193 pp.
Lee, C.T.A., Luffi, P., Plank, T., Dalton, H., Leeman, W.P., 2009. Constraints on the depths and temperatures of basaltic magma generation on Earth and other terrestrial planets using new thermobarometers for mafic magmas. Earth Planet. Sci. Lett. 279 (1–2), 20–33.
Lehnert, K., Su, Y., Langmuir, C.H., Sarbas, B., Nohl, U., 2000. A global geochemical database structure for rocks. Geochem. Geophys. Geosyst. 1, 1012.
Marsh, B.D., 1988. Crystal size distribution (CSD) in rocks and the kinetics and dynamics of crystallization I. Theory. Contrib. Miner. Petrol. 99, 277–291.
Martin, A.P., Price, R.C., Cooper, A.F., McCammon, C.A., 2015. Petrogenesis of the rifted southern Victoria Land lithospheric mantle, Antarctica, inferred from petrography, geochemistry, thermobarometry and oxybarometry of peridotite and pyroxenite xenoliths from the Mount Morning eruptive Centre. J. Petrol. 56 (1), 193–226.
McGarvie, D.W., Macdonald, R., Pinkerton, H., Smith, R.L., 1990. Petrogenetic evolution of the Torfajökull volcanic complex, Iceland II. The role of magma mixing. J. Petrol. 31 (2), 461–481.
Morgan, D.J., Jerram, D.A., 2006. On estimating Crystal Shape for Crystal size distribution Analysis. J. Volcanol. Geotherm. Res. 154, 1–7.
Moscati, R.J., Hughes, A.L., 2024. *Þingmúli Volcanic complex, eastern Iceland: Pb, Sr, and Nd isotopic data, 2024*: U.S. Geol. Surv. Data Release. https://doi.org/10.5066/P13NQWAA.
Mutch, E.J.F., Maclennan, J., Edmonds, M., 2017. December. Timing magma migration through the Icelandic Crust: from the Moho to the surface. In AGU fall meeting Abstracts (Vol. 2017, V54B-02).
Ofeigsson, B.G., Hooper, A., Sigmundsson, F., Sturkell, E., Grapenthin, R., 2011. Deep magma storage at Hekla volcano, Iceland, revealed by InSAR time series analysis. J. Geophys. Res. 116, B05401. https://doi.org/10.1029/2010JB007576.
Olive, V., Ellam, R.M., Wilson, L., 2001. A protocol for the determination of the rare earth elements at picomole level in rocks by ICP-MS: results on geological reference materials USGS PCC-1 and DTS-1. Geostand. Newslett. 25, 219–228. https://doi.org/10.1111/j.1751-908x.2001.tb00597.x.
Prestvik, T., Goldberg, S., Karlsson, H., Grönvold, K., 2001. Anomalous strontium and lead isotope signatures in the off-rift Öræfajökull central volcano in south-East

Iceland. Evidence for enriched endmember(s) of the Iceland mantle plume? Earth Planet. Sci. Lett. 190, 211–220.
Qi, Y., Gou, G.N., Wang, Q., Wyman, D.A., Jiang, Z.Q., Li, Q.L., Zhang, L., 2017. Cenozoic mantle composition evolution of southern Tibet indicated by Paleocene (~ 64 Ma) pseudoleucite phonolitic rocks in Central Lhasa terrane. Lithos 302, 178–188.
Reubi, O., Blundy, J., 2009. A dearth of intermediate melts at subduction zone volcanoes and the petrogenesis of arc andesites. Nature 461 (7268), 1269–1273. https://doi.org/10.1038/nature08510.
Rhodes, J.M., Dawson, J.B., 1975. Major and trace element chemistry of peridotite inclusions from the Lashaine volcano, Tanzania. In: Physics and Chemistry of the Earth. Pergamon, pp. 545–557.
Rollinson, H., 1993. Using geochemical data. Evaluation, presentation, interpretation. Longman Scientific and Technical, Wiley, New York, p. 352p.
Schindelin, J., Arganda-Carreras, I., Frise, E., Kaynig, V., Longair, M., Pietzsch, T., Cardona, A., 2012. Fiji: an open-source platform for biological-image analysis. Nat. Methods 9 (7), 676–682. https://doi.org/10.1038/nmeth.2019.
Schmincke, H.U., Viereck, L.G., Griffin, B.J., Pritchard, R.G., 1982. Volcaniclastic rocks of the Reydarfjördur drill hole, eastern Iceland: 1. Primary features. *Journal of Geophysical Research: Solid.* Earth 87 (B8), 6437–6458.
Selbekk, R.S., Trønnes, R.G., 2007. The 1362 AD Öræfajökul eruption, Iceland: Petrology and geochemistry of large-volume homogeneous rhyolite. J. Volcanol. Geotherm. Res. 160, 42–58.
Sun, S.S., McDonough, W.F., 1989. Chemical and isotopic systematics of oceanic basalts: implications for mantle composition and processes. Geol. Soc. Lond. Spec. Publ. 42 (1), 313–345.
Suzuki, M., Sodeoka, S., Inoue, T., 2005. Structure Control of Plasma Sprayed Zircon Coating by Substrate Preheating and Post Heat Treatment. Mater. Trans. 46 (669–674). https://doi.org/10.2320/matertrans.46.669.
Sverrisdottir, G., 2007. Hybrid magma generation preceding Plinian silicic eruptions at Hekla, Iceland: evidence from mineralogy and chemistry of two zoned deposits. Geol. Mag. 144 (4), 643–659.
Thordarson, T., Höskuldsson, Á., 2022. Iceland. In: Classic Geology in Europe 3. Publishing, Harpenden, UK, Terra.
Thordarson, T., Larsen, G., 2007. Volcanism in Iceland in historical times: Volcano types, eruption styles and eruptive history. J. Geodyn. 43, 118–152.
Timms, N.E., Erickson, T.M., Pearce, M.A., Cavosie, A.J., Schmieder, M., Tohver, E., Reddy, S.M., Zanetti, M.R., Nemchin, A.A., Wittman, A., 2017. A pressure-temperature phase diagram for zircon at extreme conditions. Earth Sci. Rev. 165, 185–202. https://doi.org/10.1016/j.earscirev.2016.12.008.
Tuttle, O.F., Bowen, N.L., 1958. Origin of granite in the light of experimental studies in the system $NaAlSi_3O_8$-$KAlSi_3O_8$-SiO_2-H_2O. Geol. Soc. Am. Memoir 74.
van Andel, T.H., Bowin, C.O., 1968. Mid-Atlantic ridge between 22° and 23° north latitude and the tectonics of mid-ocean rises. J. Geophys. Res. 73 (4), 1279–1298.
van der Meer, Q.H., Bali, E., Guðfinnsson, G.H., Kahl, M., Rasmussen, M.B., 2021. Warm and slightly reduced mantle under the off-rift Snæfellsnes Volcanic Zone, Iceland. J. Petrol. 62 (12). https://doi.org/10.1093/petrology/egab057.
Vaselli, O., Downes, H., Thirlwall, M., Dobosi, G., Coradossi, N., Seghedi, I., Szakacs, A., Vannucci, R., 1995. Ultramafic xenoliths in Plio-Pleistocene alkali basalts from the Eastern Transylvanian Basin: depleted mantle enriched by vein metasomatism. J. Petrol. 36 (1), 23–53.
Viccaro, M., Nicotra, E., Urso, S., 2015. Production of mildly alkaline basalts at complex ocean ridge settings: Perspectives from basalts emitted during the 2010 eruption at the Eyjafjallajökull volcano, Iceland. J. Geodyn. 91, 51–64.
Volk, O., White, R.S., Pilia, S., Green, R.G., Maclennan, J., Rawlinson, N., 2021. Oceanic crustal flow in Iceland observed using seismic anisotropy. Nat. Geosci. 14 (3), 168–173.
Walker, G.P.L., 1957. Geology of the Reyðarfjörður area, Eastern Iceland. Q. J. Geol. Soc. 114, 367–391.
Walker, G.P.L., 1966. Acid volcanic rocks in Iceland. Bull. Volcanol. 29 (1), 375–402.
Wilson, B.M., 1989. Igneous Petrogenesis: A Global Tectonic Approach. Unwin Hyman, London, p. 466.
Wilson, S.A., 1997. The collection, preparation and testing of USGS reference material BCR-2, Columbia River Basalt. In: U.S. Geological Survey Open-File Report 98-00x.
Zierenberg, R.A., Schiffman, P., Barfod, G.H., Lesher, C.E., Marks, N.E., Lowenstern, J.B., Mortensen, A.K., Pope, E.C., Bird, D.K., Reed, M.H., Friðleifsson, G.Ó., 2013. Composition and origin of rhyolite melt intersected by drilling in the Krafla geothermal field, Iceland. Contri. Miner. Petrol. 165 (2), 327–347.
Zimmer, M.M., Plank, T., Hauri, E.H., Yogodzinski, G.M., Stelling, P., Larsen, J., Singer, B., Jicha, B., Mandeville, C., Nye, C.J., 2010. The role of water in generating the calc-alkaline trend: new volatile data for Aleutian magmas and a new tholeiitic index. J. Petrol. 51 (12), 2411–2444.
Zindler, A., Hart, S., 1986. Chemical geodynamics. Annu. Rev. Earth Planet. Sci. 14, 493–571.